

1 **Carbon Monoxide Climatology derived from the Trajectory Mapping of**  
2 **Global MOZAIC-IAGOS Data**

3 | M. K. Osman<sup>1,\*</sup>, D.W. Tarasick<sup>1</sup>, J. Liu<sup>2,5</sup>, O. Moeini<sup>1</sup>, V. Thouret<sup>3</sup>, V. E. Fioletov<sup>1</sup>, M.  
4 Parrington<sup>4</sup>, P. Nédélec<sup>3</sup>

5 <sup>1</sup>Environment Canada, 4905 Dufferin Street, Downsview, ON, M3H 5T4 Canada

6 <sup>2</sup>Department of Geography and Program in Planning, University of Toronto, 100 St. George  
7 Street, Toronto, Ontario, M5S 3G3, Canada

8 <sup>3</sup>Laboratoire d'Aérodologie, UMR5560, CNRS and Université de Toulouse, Toulouse, France

9 <sup>4</sup>European Centre for Medium-Range Weather Forecasts, Shinfield Park, Reading, RG2 9AX,  
10 UK

11 <sup>5</sup>[School of Atmospheric Sciences, Nanjing University, Nanjing, 210023, China](#)

12 \*[Current affiliation](#): Cooperative Institute for Mesoscale Meteorological Studies, The University  
13 of Oklahoma, and NOAA/National Severe Storms Laboratory, Norman, Oklahoma, USA

14

15 **Abstract**

16 A three-dimensional gridded climatology of carbon monoxide (CO) has been developed by  
17 trajectory mapping of global MOZAIC-IAGOS in situ measurements from commercial aircraft  
18 data. CO measurements made during aircraft ascent and descent, comprising nearly 41,200  
19 profiles at 148 airports worldwide from December 2001 to December 2012 are used. Forward  
20 and backward trajectories are calculated from meteorological reanalysis data in order to map the  
21 CO measurements to other locations, and so to fill in the spatial domain. This domain-filling  
22 technique employs 15,800,000 calculated trajectories to map otherwise sparse MOZAIC-IAGOS  
23 data into a quasi-global field. The resulting trajectory-mapped CO dataset is archived monthly  
24 from 2001-2012 on a grid of 5° longitude×5° latitude×1 km altitude, from the surface to 14 km  
25 altitude.

26 | The mapping product has been carefully evaluated, ~~first~~[firstly](#) by comparing maps constructed  
27 using only forward trajectories and using only backward trajectories. The two methods show  
28 similar global CO distribution patterns. The magnitude of their differences is most commonly  
29 | 10% or less, and found to be less than 30% for almost all cases. [Secondly](#), ~~t~~[the](#) method has ~~also~~  
30 been validated by comparing profiles for individual airports with those produced by the mapping  
31 method when data from that site are excluded. While there are larger differences below 2 km, the  
32 two methods agree very well between 2 and 10 km with the magnitude of biases within 20%.  
33 Finally, the mapping product is compared with global MOZAIC-IAGOS cruise-level data, which

1 were not included in the trajectory-mapped dataset, and with independent data from the NOAA  
2 aircraft flask sampling program. [The trajectory-mapped MOZAIC-IAGOS CO values show](#)  
3 [generally good agreement with both independent data sets.](#)

4 Maps are also compared with Version 6 data from the Measurements Of Pollution In The  
5 Troposphere (MOPITT) satellite instrument. Both data sets clearly show major regional CO  
6 sources such as biomass burning in central and southern Africa and anthropogenic emissions in  
7 eastern China. While the maps show similar features and patterns, and relative biases are small in  
8 the lowermost troposphere, we find differences of ~20% in CO volume mixing ratios between  
9 500 hPa and 300 hPa. These upper troposphere biases are not related to the mapping procedure,  
10 as almost identical differences are found with the original in situ MOZAIC-IAGOS data. The  
11 total CO trajectory-mapped MOZAIC-IAGOS column is also higher than the MOPITT CO total  
12 column, by 12-16%.

13 The dataset shows the seasonal CO cycle over different latitude bands and altitude ranges as well  
14 as long-term trends over different latitude bands. We observe a decline in CO over the northern  
15 hemisphere extratropics and the tropics consistent with that reported by previous studies using  
16 other data sources.

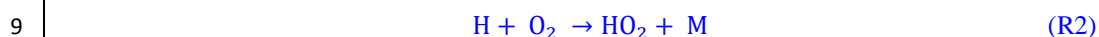
17 We anticipate use of the trajectory-mapped MOZAIC-IAGOS CO dataset as an a priori  
18 climatology for satellite retrieval, and for air quality model validation and initialization.

## 19 **1 Introduction**

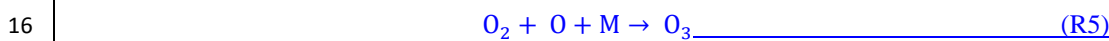
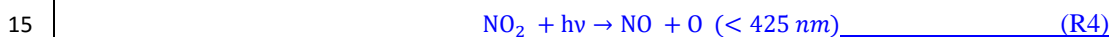
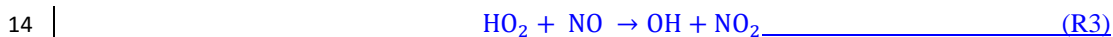
20 Atmospheric carbon monoxide (CO) is an important global air pollutant and trace gas. Due to its  
21 relatively long lifetime of 1-4 months (Hubler et al., 1992; Law and Pyle, 1993), it is an ideal  
22 tracer for long range atmospheric transport (Logan et al., 1981; Lelieveld et al., 2001; Shindell et  
23 al., 2006). Moreover, in the tropics, it is an important tracer of upward transport during  
24 convective events (e.g., Pommrich et al., 2014). Consequently, it has been employed to facilitate  
25 interpretations of chemical measurements (Jaffe et al., 1996; Parrish et al., 1991, 1998; Wang et  
26 al., 1996, 1997) and in validating chemical transport models (Carmichael et al, 2003; Liu et al.,  
27 2003; Tan et al., 2004; Wang et al., 2004). The main sources of atmospheric CO are relatively  
28 well understood (Galanter et al., 2000; Granier et al., 2011; Holloway et al., 2000); however, the  
29 magnitude of individual sources and their seasonal variability, especially of biomass burning, are  
30 not well quantified. Stein et al. (2014) also reported that models are also generally biased low  
31 due to either an underestimation of CO sources or an overestimation of its sinks. There are  
32 differences in the emission densities of anthropogenic and natural sources, despite the fact that  
33 the anthropogenic and natural sources are of similar magnitude on a global scale (Granier et al.,  
34 2011; Logan et al., 1981). The anthropogenic sources are primarily associated with large  
35 industrial centers or major biomass burning regions while the natural sources, such as oxidation  
36 of methane (CH<sub>4</sub>) and non-methane hydrocarbons (NMHCs) are much more diffuse. This makes

1 CO a good atmospheric tracer gas for anthropogenic emissions as its lifetime allows it to be used  
2 as an indicator of how large-scale atmospheric transport redistributes pollutants on a global scale.

3 CO plays a vital role in the chemistry of the atmosphere. This significance mainly comes from  
4 the influence of CO on the concentrations and distributions of the atmospheric oxidants, ozone  
5 ( $O_3$ ), the hydroperoxy ( $HO_2$ ) and hydroxyl radicals (OH) (e.g. Novelli et al., 1994, 1998).  
6 Reaction (R1) between CO and OH represents 90-95% of the CO sink (Logan et al., 1981), and  
7 about 75% of the removal of OH (Thompson, 1992) in the troposphere:



10 In areas with sufficient  $NO_x$  ( $=NO + NO_2$ ),  $HO_2$  formed in reaction (R2) leads to photochemical  
11 reactions (R3)-(R5) which bring about net  $O_3$  production. In urban areas and regions of biomass  
12 burning, large amounts of these  $O_3$  precursors will be produced, and  $O_3$  can be formed in, and  
13 downwind of, the source region (Crutzen, 1973; Fishman and Seiler, 1983):



17  $O_3$  is associated with respiratory problems and decreased crop yields (e.g., McKee, 1993;  
18 Chameides et al., 1994). Since CO and OH are principal reaction partners, CO concentrations in  
19 the atmosphere have important climatological implications. OH is also responsible for the  
20 removal of greenhouse gases such as  $CH_4$ , and other volatile organic compounds in the  
21 atmosphere. Via these interactions with OH,  $O_3$  and  $CH_4$ , CO has an indirect radiative forcing of  
22 about  $0.25 \text{ W m}^{-2}$  (IPCC AR5).

23 Global atmospheric chemistry models require accurate CO concentrations on a global scale in  
24 order to define spatial and temporal variations of atmospheric oxidants and CO. For this reason  
25 measurements of CO are made by different kinds of remote sensing and in situ instruments, in  
26 ground-based networks, aircraft programmes and from space (Novelli et al., 1994, 1998;  
27 Rinsland and Levine, 1985; Zander et al., 1989; Brook et al., 2014; Reichle et al., 1990; 1999;  
28 Worden et al., 2013; Petzold et al., 2015). Long range atmospheric transport redistributes CO  
29 widely due to its relatively long lifetime. Typical tropospheric background CO levels range  
30 between 50 and 120 ppbv (WHO, 2000). Mixing ratios much higher than 250 ppb have been  
31 observed in the upper troposphere over Asia (Nédélec et al., 2005) or over the Pacific (Clark et  
32 al., 2015) in biomass burning plumes. CO values as high as 1800 ppbv have been reported over  
33 Beijing (Zbinden, et al., 2013)

1 Early studies of ground-based observations showed increasing trends in global CO before 1980  
2 (Khalil and Rasmussen, 1988; Rinsland and Levine, 1985; Zander et al., 1989), followed by a  
3 modest decline in the 1990s (Novelli et al. 1994; 2003; Khalil and Rasmussen, 1994). More  
4 recently satellite observations have shown that the decline has continued: Worden et al. (2013)  
5 report a global trend from 2000-2011 of ~10% per decade on column CO in the northern  
6 hemisphere. Petetin et al. (2015) show a similar decrease of about 2 ppb per year over Frankfurt  
7 throughout the troposphere from 2002 to 2012. The decrease is at least partly due to a decrease in  
8 global anthropogenic CO emissions (Granier et al., 2011).

9 **In-service Aircraft for a Global Observing System (IAGOS), and its predecessor Measurement**  
10 **of Ozone and water vapor by Airbus in-service airCraft (MOZAIC), have been making**  
11 **automatic and regular measurements of O<sub>3</sub>, water vapour and standard meteorological**  
12 **parameters onboard long-range commercial Airbus A340 aircraft since August 1994 (Marengo et**  
13 **al., 1998, Petzold et al., 2015). Measurements of CO (Nédélec et al., 2003) and NO<sub>y</sub> (the sum of**  
14 **NO<sub>x</sub> plus its atmospheric oxidation products) (Volz-Thomas et al., 2005) were added in late**  
15 **2001. The MOZAIC database currently contains data from more than 41,200 vertical profiles of**  
16 **CO, measured during takeoff and landing from 148 airports around the world. MOZAIC**  
17 **measurements show the general features of the atmospheric CO distribution (Zbinden et al.,**  
18 **2013; Petzold et al., 2015 and references therein), capturing major regional features (e.g., strong**  
19 **CO emissions from biomass burning or anthropogenic sources).**

20 The objective of this paper is to present a three-dimensional (i.e., latitude, longitude, altitude)  
21 gridded climatology of carbon monoxide that has been developed by trajectory mapping of  
22 global MOZAIC-IAGOS CO data from 2001-2012. We employ a domain-filling technique,  
23 using approximately 15,800,000 calculated trajectories to map otherwise sparse MOZAIC-  
24 IAGOS CO data into a global field.

25 This is a technique that has been used successfully with tropospheric and stratospheric  
26 ozonesonde data (G. Liu et al., 2013; J. Liu et al., 2013). Stohl et al. (2001) used trajectory  
27 statistics to extend one year of MOZAIC O<sub>3</sub> measurements into a 4-season O<sub>3</sub> climatology at 10°  
28 longitude by 6° latitude and three vertical heights. Tarasick et al. (2010) developed high  
29 resolution (1°×1°×1 km in latitude, longitude, and altitude) tropospheric O<sub>3</sub> fields for North  
30 America from ozonesonde data from the INTEX (Intercontinental Transport Experiment) and  
31 ARCTAS (Arctic Research of the Composition of the Troposphere from Aircraft and Satellites)  
32 campaigns, and this was extended to global tropospheric ozonesonde data by G. Liu et al. (2013).  
33 It is possible to apply this technique to CO because the lifetime of CO in the troposphere, as  
34 noted above, is generally of the order of weeks or months. This physically-based method, using  
35 the reanalysis meteorological data from the National Centers for Environmental  
36 Prediction/National Center for Atmospheric Research (NCEP/NCAR) (Kalnay et al., 1996) to, in  
37 effect, interpolate data based on knowledge of atmospheric transport, offers obvious advantages  
38 over typical statistical interpolation methods.

1 **2 Measurements of CO**

2 **2.1 MOZAIC-IAGOS**

3 CO measurements were made by an improved version of a commercial Model 48CTL CO  
4 Analyzer from Thermo Environmental Instruments employing the Gas Filter Correlation  
5 technique. The Model 48CTL is based on the principle that CO absorbs infrared radiation at a  
6 wavelength of 4.67 microns. For 30 s integration time (the response time of the instrument) the  
7 precision achieved is 5 ppb (noise) or 5% (calibration) CO, with minimum detection limit of 10  
8 ppb. The analyzer samples at a horizontal resolution of about 7 km (since the maximum cruise  
9 speed of the Airbus A340 aircraft is nearly 250 m/s) and the vertical resolution during ascents  
10 and descents is nearly 300 m. Nedelec et al. (2003 for MOZAIC, 2015 for IAGOS) give detailed  
11 descriptions of the CO analyzer, measurement technique, instrument validation and quality  
12 testing.

13 The airports visited by aircraft equipped with MOZAIC-IAGOS instrumentation are shown in  
14 Fig. 1. Further details are available at <http://www.iagos.fr>.

15

16

17 **Fig. 1.** Airports visited by MOZAIC-IAGOS aircraft from 2001-2012. The color bar indicates  
18 the number of profiles available from each airport. The squares show the locations of the selected  
19 airports used for the validation in this study.

20 The sampled data from these airports are unevenly distributed spatially, and also temporally  
21 because the frequency of visits to airports by aircraft that take part in MOZAIC-IAGOS varies  
22 considerably depending on commercial airlines' operational constraints. Thus at Frankfurt,  
23 Germany we find 12,324 CO profiles while from Dammam, Saudi Arabia we have only 2 during  
24 the period 2001-2012. The trajectory-mapping method is valuable for filling the sparse and  
25 variable spatial domain.

26 **2.2 MOPITT**

27 MOPITT is a nadir-viewing gas correlation radiometer which provides global atmospheric  
28 profiles of CO volume mixing ratio (VMR) and CO total column values using near-infrared  
29 radiation at 2.3  $\mu\text{m}$  and thermal-infrared radiation at 4.7  $\mu\text{m}$  (Drummond and Mand, 1996). CO  
30 columns and profiles are retrieved from the IR emission channels (4.6  $\mu\text{m}$ ) for all cloud-free  
31 scenes. The MOPITT measurement technique relies on a temperature gradient within the  
32 atmosphere, leading to a retrieval dependence on surface temperature, and little sensitivity to CO  
33 in the boundary layer. The retrieval uses a priori profiles that vary geographically and  
34 temporally. MOPITT-derived CO VMR profiles reflect the vertical sensitivity of the  
35 measurement as defined by the retrieval averaging kernel (e.g. Fig. 3) and a priori profile. In this

1 study, we have used Level 3, Version 6 monthly CO mixing ratio profile data, reported on 10  
2 pressure levels, as well as CO total column. Nighttime CO observations of MOPITT have not  
3 been validated and appear subject to larger bias (Heald et al., 2004). Hence, we use the daytime  
4 data for comparison. MOPITT data are publicly available at the NASA Langley Research Center  
5 Atmospheric Science Data Center: [https://eosweb.larc.nasa.gov/project/mopitt/mopitt\\_table](https://eosweb.larc.nasa.gov/project/mopitt/mopitt_table).

6 MOPITT was launched in 1999 into sun-synchronous polar orbit with a 1030 local time (LT)  
7 northward or southward equator cross-over time. The instrument field of view is 22x22 km<sup>2</sup>.  
8 Cross-track scanning with a 612 km swath provides near complete coverage of the surface of the  
9 Earth approximately every 3 days. MOPITT retrievals have gone through intensive validation  
10 against in situ measurements from aircraft on a regular basis since the start of the mission  
11 (Worden et al., 2010; Deeter et al., 2012, 2013, 2014; Emmons et al., 2004, 2007, 2009; Jacob et  
12 al., 2003). MOPITT CO retrievals have also been validated by comparing to ground-based and  
13 TES satellite measurements (Jacob et al., 2003 and Luo et al., 2007). Deeter et al. (2014) employ  
14 the MOPITT L3 V6 product and show biases to vary from -5.2% at 400 hPa to 8.9% at the  
15 surface. Previous studies used earlier versions of the MOPITT product.

### 16 **2.3 Trajectory calculation and global CO mapping via HYSPLIT**

17 For each CO profile of the MOZAIC-IAGOS data set presented here, the mean CO VMR was  
18 calculated for 1-km intervals from sea level up to 12 km (the maximum altitude of the aircraft).  
19 Cruise data were not used. The HYSPLIT (Hybrid Single-Particle Lagrangian Integrated  
20 Trajectory) model version 4.9 (Draxler and Hess, 1998, Draxler, 1999) was employed to  
21 calculate trajectories for each level of each profile. The exact location of the aircraft was used to  
22 start the trajectories. HYSPLIT, publicly accessible at <http://ready.arl.noaa.gov/HYSPLIT.php>, uses  
23 the reanalysis meteorological wind fields from the National Centers for Environmental  
24 Prediction/National Center for Atmospheric Research (NCEP/NCAR) (Kalnay et al., 1996) as an  
25 input to describe the transport of CO in the atmosphere. The reanalysis data are available from  
26 1948 until the present. Both forward and backward trajectories for 4 days at 6-hour intervals (32  
27 positions for each level) were calculated for 41,200 CO profiles, and the mean CO mixing ratios  
28 from each level (i.e., tropospheric and lower stratospheric air masses) of each profile were  
29 assigned to the corresponding trajectory positions along the forward and backward paths.  
30 Trajectories only move upward and downward with the meteorological vertical velocity fields  
31 since the HYSPLIT kinematic trajectory model employs vertical motions supplied with the  
32 NCEP reanalysis meteorological data set. Numerous studies show that the choice of vertical  
33 wind velocity has significant impact on the transport of tracers (e.g., Schoeberl et al. 2003;  
34 Ploeger et al., 2010, 2012). Kinematic models show excessive dispersion for tracers with strong  
35 gradients (e.g., O<sub>3</sub> in the vicinity of the tropopause), particularly for trajectories of 7 days or  
36 more. Here trajectories were limited to a maximum of 4 days in length. Moreover, unlike O<sub>3</sub>, CO  
37 does not have a strong vertical gradient in the upper troposphere. Trajectories that reach the  
38 ground continue at the surface where trajectory robustness is more uncertain. Trajectories that  
39 reach the top height of the model (20,000 m above sea level) terminate. Although HYSPLIT is

1 capable of generating a trajectory every hour (i.e., 24 trajectories per day), the typical maximum  
2 frequency of CO measurements is around 2 profiles per day (with the exception of Frankfurt  
3 where we can get up to 6 profiles per day). In this version, no attempt was made to identify  
4 individual CO sources; however, the climatology could in principle be refined by excluding back  
5 trajectories from sources identified via emission inventories. We note, however, that if major  
6 anthropogenic sources were a significant source of error, we would see differences between the  
7 CO mapping produced using only backward and only forward trajectories (see Sect. 3.1).

8 This mapping implicitly assumes that CO chemistry may be neglected over a timescale of 4 days.  
9 Except near major sources, this assumption should be valid, as the lifetime of CO is much  
10 longer. However, trajectories have significant errors over such timescales. Stohl (1998) in a  
11 comprehensive review, quotes typical errors of about 100-200 km/day in the troposphere. This  
12 can be combined with an estimate of the correlation length in the troposphere to yield an estimate  
13 for the information value of a mapped measurement. Liu et al. (2009) find that O<sub>3</sub> measurements  
14 in the troposphere correlate with an exponential dependence of approximately  $e^{-(r/R)^{1.5}}$ , where  $r$   
15 is distance and  $R$  is a correlation length of 500-1000 km in the troposphere, and 1000-2000 km in  
16 the stratosphere. As the CO lifetime is even longer than the ozone lifetime, the correlation length  
17 for CO should be at least as large. Therefore, the trajectory-mapped data were binned at intervals  
18 of 5° latitude and 5° longitude, at every 1-km altitude, and averaged with a weighting,  $w$ ,  
19 assigned according to the formula:

$$20 \quad w = e^{-(150t/R)^{1.5}} \quad (1)$$

21 where  $R$  is the correlation length (taken as 700 km in the troposphere and 1500 km in the  
22 stratosphere), and  $t$  is the age of the trajectory in days.

23 The trajectory mapping greatly spreads out the in situ CO information along the trajectory paths,  
24 increasing the spatial domain to include much of the globe. Two different vertical coordinate  
25 systems were utilized for the binning, and hence the maps were generated for elevations above  
26 sea level and above ground level. Data are available publicly at [ftp://es-ee.tor.ec.gc.ca/pub/ftpd/MOZAIC\\_output\\_CO/](ftp://es-ee.tor.ec.gc.ca/pub/ftpd/MOZAIC_output_CO/). In this work, we present global CO maps generated  
27 for elevations above sea level. Global maps of monthly, annual, seasonal and decadal means are  
28 presented, for each altitude, from 2001-2012.

#### 30 **2.4 Distribution of data and uncertainties associated with trajectory mapping**

31 Figure 2 shows typical standard errors of the mapping product and the number of samples per  
32 grid cell, for typical monthly, annual and decadal maps at 4.5 km altitude above sea level.  
33 Similar figures for other levels are included with the climatology on the FTP site. As can be  
34 seen, the largest number of samples per grid cell and the lowest standard errors are found over  
35 North America and Europe as there are more frequent MOZAIC-IAGOS aircraft flights in this  
36 region. Higher standard errors are found at NH high latitudes and much of the SH, where airports  
37 visits by MOZAIC-IAGOS-equipped aircraft are much fewer. The standard error is computed

1 using all data points found inside a grid cell. This is probably biased low, since some grid cells  
 2 may contain more than one value from a particular trajectory. This bias is likely not more than a  
 3 factor of 2, based on typical trajectory lengths. These maps present a visual interpretation that  
 4 distinguishes regions where the CO climatology is 'statistically robust' (for example, North  
 5 America and Europe) from those regions where the uncertainty is larger. The average number of  
 6 samples is approximately 20, 90, and 140 per grid cell for the monthly, annual and decadal maps,  
 7 and this number does not vary greatly among layers. The average standard error is generally  
 8 between 3 and 4% of the mean at 4.5 km for all three averaging periods. The monthly mean  
 9 shows the highest error and the lowest number of samples per grid cell.

10 Fig. 2 The standard error of the mean (left panels) and number of samples (right panels) for  
 11 monthly (July 2012), annual (2005), seasonal (DJF 2001-2012) means at 4.5 km altitude above  
 12 sea level. The month and year shown are chosen as typical; other months and years show similar  
 13 patterns. The data are binned on a 5°×5° latitude and longitude grid.

## 14 2.5 MOZAIC-IAGOS Comparison with MOPITT

15 When comparing the MOPITT retrievals with in situ data, it is necessary to take into account the  
 16 sensitivity of the retrievals to the true profiles. The method used by MOPITT to retrieve  
 17 tropospheric CO profiles follows that of Rodgers (2000). In order to perform the most  
 18 meaningful and accurate comparison, the in situ data to be compared must be transformed using  
 19 the averaging kernel matrix,  $A$ , and a priori profile,  $x_a$ , as shown by Eq. (2). A “retrieved”  
 20 comparison profile,  $x_{ret}$ , is calculated by using the in situ profile,  $x$ , as the “true” profile in  
 21 Eq. (2) which is interpolated to the lower resolution of MOPITT. As described by Emmons et al.  
 22 (2004), the in situ profile ( $x$ ) is transformed with averaging kernel matrix ( $A$ ) and the a priori CO  
 23 profile ( $x_a$ ) to get a profile ( $x_{ret}$ ), the appropriate quantity to compare with the MOPITT  
 24 retrievals:

$$25 \quad x_{ret} = x_a + A(x - x_a) + \varepsilon = Ax + (I - A)x_a + \varepsilon \quad (2)$$

26 where  $I$  is the identity matrix and  $\varepsilon$  is the retrieval error due to random errors in the  
 27 measurement and systematic errors in the forward model (e.g., the error in the atmospheric  
 28 temperature retrieval).  $x_{ret}$ ,  $x$ , and  $x_a$  are expressed in terms of the logarithm of the VMR.  
 29 The averaging kernels provide the relative weighting between the true and a priori profiles and  
 30 reflect the sensitivity of the retrieval to the measurement (Worden et al., 2013). They are very  
 31 sensitive to the surface temperature and will be different for each point on the globe. The matrix  
 32  $A$  describes the sensitivity of the retrieved CO log(VMR) profile to perturbations applied at each  
 33 level of the “true” log(VMR) profile. The quantity  $x_{ret}$ , the transformed in situ profile,  
 34 represents the result of applying a linear transformation to the in-situ profile in the same way that  
 35 the remote sensing retrieval process is believed to transform the true profile. Thus,  $x_{ret}$  can be  
 36 directly compared against the MOPITT retrieved CO profile in a manner that is not affected by  
 37 varying vertical resolution or a priori dependence. The vertical resolution of the retrieved profile



1 is described by the shapes of the averaging kernels. Figure 3 shows that the kernels are broad  
 2 except at pressure levels between 400-300 hPa and exhibit a large degree of overlap. The overlap  
 3 of the averaging kernels peaking in the boundary layer and those at the top of the atmosphere  
 4 indicates a significant correlation for the retrieved values at these levels. Typical full-width at  
 5 half maximum (FWHM) of these curves is approximately 5-8 km. The retrieved CO values at  
 6 both top and bottom are also influenced by CO at mid levels, and by the a priori CO profile at all  
 7 pressure levels. The averaging kernels also describe the relative contributions, to the CO VMR  
 8 retrieved at a given level, of the true and a priori (via I - A) CO profiles at all pressure levels (Eq.  
 9 (2)). Where the area under the averaging kernel is smaller, the a priori information in the  
 10 retrieved CO profile is relatively larger. MOPITT CO averaging kernels exhibit variability from  
 11 month to month, season to season as well as nighttime to daytime, depending on the atmospheric  
 12 temperature profile, surface pressure and the CO profile itself.

13 The vertical coordinate of the MOZAIC-IAGOS climatology profile is kilometers above sea  
 14 level, while the MOPITT a priori profile and averaging kernels are on pressure levels in hPa.  
 15 Therefore, before applying the MOPITT averaging kernels the climatology data were  
 16 interpolated using NCEP global pressure profiles that vary as a function of time (month) and  
 17 latitude, to the 10 vertical pressure grid levels (1000, 900, 800, 700, 600, 500, 400, 300, 200, and  
 18 100 hPa) used by MOPITT. The interpolated profile was then convolved with the a priori profile  
 19 and the averaging kernels following Eq. (2) (Emmons et al., 2004). For the atmospheric residual  
 20 above the maximum MOZAIC-IAGOS profile altitude, the MOPITT a priori profiles were used.

21 In order to compare with these transformed CO profiles, the MOPITT CO profiles, averaging  
 22 kernels, and a priori profiles were mapped down from the original horizontal resolution of  $1^\circ \times 1^\circ$   
 23 in latitude and longitude to a reduced  $5^\circ \times 5^\circ$  grid. Two examples of comparisons of trajectory-  
 24 mapped MOZAIC-IAGOS CO profiles with individual (reduced)  $5^\circ \times 5^\circ$  MOPITT CO profiles are  
 25 shown in Fig. 3. The application of the averaging kernels to the MOZAIC-IAGOS CO profile  
 26 results in a vertical transformation which can shift mixing ratios significantly at some levels. The  
 27 averaging kernel, for example, identified as "1000" (i.e., surface) shows how changes to the true  
 28 CO mixing ratio at all ten retrieval levels would each contribute to a change in the retrieved  
 29 value at the surface at 1000 mbar. The original trajectory-mapped MOZAIC-IAGOS climatology  
 30 profile is quite different from the transformed climatology profile and the departures of the  
 31 transformed CO mixing ratio from the true mixing ratios can be as large as 60 ppb at some  
 32 pressure levels.

33 CO total column amounts are retrieved from the MOPITT observations in addition to the profile  
 34 retrievals. The retrieved CO total column  $c_{ret}$  (a scalar) is related to the retrieved profile  $x_{ret}$  (a  
 35 vector) through the linear relation

$$36 \quad c_{ret} = \mathbf{t}^T \mathbf{x}_{ret} \quad (3)$$

1 where T indicates the transpose operation and  $\mathbf{t}$  is the total column vectors. The CO total column  
2 averaging kernel can be calculated from the profile averaging kernels by

$$3 \quad \mathbf{a} = \mathbf{t}^T \mathbf{A} \quad (4)$$

4 The column operator simply converts the mixing ratio for each retrieval level to a partial column  
5 amount. Using the hydrostatic relation, the operator  $\mathbf{t}$  is expressed as

$$6 \quad \mathbf{t} = 2.120 \cdot 10^{13} \Delta p \quad (5)$$

7 Equation (5) is expressed in molecules/cm<sup>2</sup>/ppbv and  $\Delta p$  is the vector of the thicknesses of the  
8 retrieval pressure levels (in hPa).

9 **Fig. 3.** Examples of comparisons of monthly means of the trajectory-mapped MOZAIC-IAGOS  
10 CO profiles, with the corresponding MOPITT averaging kernels, a priori and retrievals. The left  
11 panels of each subplot show the original trajectory-mapped MOZAIC-IAGOS climatology  
12 profile (green, i.e. unsmoothed), the a priori profile, the transformed trajectory-mapped  
13 MOZAIC-IAGOS climatology profile (red, i.e. smoothed), and the MOPITT retrieved CO  
14 profile. The right panel show the mean averaging kernels, for different pressure levels, obtained  
15 by averaging all daytime averaging kernels in the 5°x5° latitude-longitude box centered on the  
16 coordinates indicated.

### 17 **3 Validation**

18 Validation of the trajectory-mapped MOZAIC-IAGOS CO dataset product has been performed  
19 by (1) comparing maps constructed using only forward trajectories against those constructed  
20 using only backward trajectories; (2) comparing profiles for individual airports against those  
21 produced by the mapping method when data from that site are excluded; (3) comparing with  
22 global MOZAIC-IAGOS cruise-level data, which were not included in the trajectory-mapped  
23 dataset, and (4) comparing with independent data from the NOAA aircraft flask sampling  
24 program.

#### 25 **3.1 Comparison of trajectory-mapped MOZAIC-IAGOS CO profiles**

26 As a first step in validation of the trajectory-mapped climatology, Figs. 4 and S1 assess the  
27 differences between the CO mapping produced using only backward and only forward  
28 trajectories for different seasons using the 7.5 km level as an example. If chemistry (i.e. local  
29 sources or sinks) were a significant source of error then one would expect to see differences  
30 between these maps. In fact, the CO distribution patterns are very similar (Fig. 4). Differences  
31 are most commonly 10% or less, and found to be less than 30% for almost all cases. They are  
32 typically less than 10% at northern mid-latitudes and less than 20% in the tropics between ±30°  
33 latitude, except in the Pacific and Atlantic oceans where they can be as large as 30%. Differences  
34 (Fig. S1) also show no distinct pattern, except for some clustering in areas where the trajectories

1 are longest, and therefore least reliable. As differences between the two distributions are  
2 comparable with the uncertainties of the mean value estimates and not systematic, it is  
3 reasonable to combine forward and backward mapped values to produce an averaged CO map.

4

5

6 **Fig. 4.** Examples of the global distribution, 2001-2012, of trajectory-mapped MOZAIC-IAGOS  
7 CO (ppbv) produced using only backward and only forward trajectories at 7.5 km a.s.l. Panels  
8 correspond to different seasons: (a, b) December-February, (c, d) March-May, (e, f) June-August  
9 and (g, h) September-November.

### 10 **3.2 Comparison between trajectory-mapped and in situ profiles**

11 A good test of an interpolation model is to examine how it performs in areas where no data are  
12 available. Figure 5 compares the trajectory-mapped climatology profiles at three airport sites  
13 (Frankfurt, Germany; Houston, USA; and Tokyo, Japan) with the average of the MOZAIC-  
14 IAGOS data from each of these sites for May of 2001-2012. Houston and Tokyo are not as well  
15 sampled as Frankfurt (Figure 1). The climatology profiles for each location were produced by  
16 excluding data from that location, but using all other MOZAIC-IAGOS data.

17 Generally, the profiles from the two methods agree very well and the agreement is especially  
18 good in the free troposphere, at altitudes between 2 and 10 km. [Referring to the bottom panels of](#)  
19 [Fig. 5,](#) [the magnitude of the differences for most altitudes is well under 20%.](#)

20

21

22 **Fig. 5.** Comparisons of trajectory-mapped MOZAIC-IAGOS CO climatology and MOZAIC-  
23 IAGOS profiles at three sites. The climatology profiles for each location were produced by  
24 excluding data from that location, but using all other MOZAIC-IAGOS data. The horizontal  
25 error bar half-length is twice the standard error of the mean (equivalent to 95% confidence limits  
26 on the averages when the number of data points is large).

27 Fig. 6 shows seasonally-averaged differences, using this method, for a number of airports with  
28 different characteristics. The airport stations that have been selected in this validation study  
29 represent tropical and northern hemisphere midlatitude locations that are subject to different  
30 meteorological and CO source conditions. Agreement is generally good in the free troposphere.  
31 There are larger differences- below 2 km where trajectories have larger errors predominantly due  
32 to complex dispersion and turbulence in the planetary boundary layer [Stohl and Seibert, 1998] .  
33 The largest differences are seen where other sources of data are distant. The smallest overall bias  
34 is seen at Frankfurt, even though the exclusion of Frankfurt data removes nearly 1/3 of the total

1 number of profiles. Apparently data from nearby airports such as Munich (Germany) and  
2 Brussels (Belgium) map accurately to the Frankfurt location. The consistency of these validation  
3 tests suggests that the trajectory-mapped dataset provides a reliable picture of the tropospheric  
4 CO distribution.

5

6 **Fig. 6.** Seasonal mean relative biases  $[2(\text{Clim-MOZAIC})/(\text{Clim+MOZAIC})]$ , expressed in %,   
7 between trajectory-mapped and MOZAIC-IAGOS in situ profiles for the period from 2001 to   
8 2012. The selected airports are representative of different meteorological and source conditions   
9 across the globe. N, lat and lon are the number of profiles, latitude and longitude of each airport.

### 10 **3.3 Comparison with the MOZAIC-IAGOS in-situ for Upper Troposphere**

11 We can also compare the trajectory-mapped profile data and MOZAIC-IAGOS in situ global CO   
12 data at cruise altitudes between 8 and 12 km. The right panels of Fig. 7 show the global seasonal   
13 mean (December-February, March-May, June-August and September-November) distribution of   
14 CO in the upper troposphere (within 60 hPa below the tropopause) for the period from 2003 to   
15 2011. Elevated CO levels in the upper troposphere are generally seen over the areas where there   
16 is strong biomass burning (central Africa, southern Africa and South America) . High CO   
17 emissions are observed over eastern China in MAM primarily due to a rise in coal use (Boden et   
18 al., 2009; Gregg et al., 2008; Tie et al., 2006) and an increasing number of vehicles (Cai and Xie,   
19 2007).

20 | The left panels of Fig. 7 –show the trajectory-mapped climatology 2001-2012 at altitudes   
21 between 7 and 9 km above sea level. The trajectory-mapping yields more data over the oceans   
22 and NH high latitudes. However, both figures show high CO values in spring in both   
23 hemispheres and elevated CO levels over regions where there are strong sources. Comparable   
24 CO values are noticeable from the figures over the Northern Atlantic Ocean, although the   
25 trajectory-mapped data appear high over high-elevation areas like Greenland and the Himalayas.   
26 | This may be due to over-correction of trajectories for terrain differences. Overall, the qualitative   
27 agreement between the trajectory-mapped CO and MOZAIC-IAGOS in situ CO cruise data   
28 appears very good, even in remote areas.

29

30

31 **Fig. 7.** Global distribution of seasonal mean trajectory-mapped MOZAIC-IAGOS CO between   
32 7-9 km altitudes above sea level for the period from 2001 to 2012. Left: MOZAIC-IAGOS   
33 trajectory. Right: MOZAIC-IAGOS cruise altitude.

### 34 **3.4 NOAA CO vertical profiles**

1 The vertical in situ CO profiles acquired through NOAA’s flask sampling program have been  
2 extensively utilized previously for validation of CO measurements of MOPITT [Emmons et al.,  
3 2004; Emmons et al., 2009; Deeter et al., 2010; Deeter et al., 2013]. Typically 12–15 flask  
4 samples are utilized to derive an in situ profile and a single flask is used to sample air at a unique  
5 altitude, providing in situ measurements from near the ground up to about 300–350 hPa. The  
6 flasks are shipped to the Global Monitoring Division of NOAA’s Earth System Research  
7 Laboratory (ESRL) for trace gas analysis. Details on procedures of sample collection are found  
8 in Novelli et al. [1992], Lang et al. [1992], and Conway et al. [1994].

9 Figure 8 shows comparisons between NOAA in-situ data and the trajectory-mapped MOZAIC-  
10 IAGOS CO climatology, for altitude ranges of 0-2, 2-4, 4-6 and 6-8 km The comparison uses all  
11 available flask data (1940 profiles for the period from 2001-2012). NOAA CO data points are  
12 matched with the corresponding grid cell ( $5^{\circ} \times 5^{\circ} \times 1$  km) of the monthly climatology, for the  
13 same year and month. If the monthly CO value for a particular grid cell is missing, the seasonal  
14 mean (if it exists) of the trajectory-mapped CO climatology (2001-2012) is used for the  
15 comparison. Above 2 km agreement is fairly good, considering that the comparison is between  
16 point measurements and monthly averages over a large volume. The positive bias below 2 km is  
17 probably due to the effect of urban sources of CO since airports are located close to cities. In  
18 general, MOZAIC-IAGOS CO measurements at takeoff and landing are above background. This  
19 “airport effect” decreases rapidly as can be from the figure for higher altitudes. This decrease is  
20 not only because the aircraft ascends above the boundary layer, but also samples over 150-400  
21 km in distance as the aircraft ascends to, or descends from, cruise altitude.

22

23

24 Fig. 8 CO mixing ratio comparison between trajectory-derived and NOAA flask data for the  
25 period from 2001-2012, for four altitude ranges. Bias is calculated as the mean of the differences  
26 in %,  $[2(\text{NOAA}-\text{Clim})/(\text{Clim}+\text{NOAA})]$ , of all data points. The blue line is the line of best fit, the  
27 red line is the 1:1 line, N is number of data pairs, and R is the correlation coefficient. Monthly  
28 trajectory mapped CO data are used for the comparison, or seasonal mean values if the monthly  
29 mean value for a particular grid cell is not available.

#### 30 **4 Trajectory-mapped MOZAIC-IAGOS Versus MOPITT**

31 This section is devoted to comparing the trajectory-mapped MOZAIC-IAGOS CO dataset with  
32 the extensively validated product from the MOPITT instrument onboard the NASA Terra  
33 satellite, which has been operating continuously since March 2000 (Drummond and Mand, 1996;  
34 Edwards et al., 1999). Global comparison is made for both CO profiles and CO total column for  
35 different time periods.

#### 36 **4.1 Comparison with MOPITT CO profiles**

1 As described in Section 2.4, in order to make a rigorous comparison with MOPITT data, the  
2 climatology profiles are first transformed using the corresponding MOPITT a priori profiles and  
3 averaging kernels via Eq. (2). Figure 3 shows examples of retrieved CO profiles ( $x_{ret}$ ), together  
4 with the original climatology ( $x$ ) and the a priori profiles ( $x_a$ ).

5 When comparing MOPITT CO retrievals and the trajectory-mapped CO profile it is useful to  
6 keep in mind the shapes and magnitudes of the averaging kernels. For example, the generally  
7 broad and weak averaging kernels for the 100 and 1000 mbar levels indicate that a significant  
8 fraction of the information in the retrieval is from the a priori profile and from other altitudes.  
9 Figure 3 also cautions that the transformed trajectory-mapped MOZAIC-IAGOS CO is closer to  
10 both the MOPITT CO retrievals and a priori profiles when there is less information from the  
11 measurement. In the lower troposphere the MOPITT CO retrieval profile is positively biased  
12 (Deeter et al., 2014), whereas the bias is negative in the upper troposphere. In Fig. 3, we have  
13 used only the dayside retrievals from MOPITT as the dayside retrievals have the maximum  
14 information content (Deeter et al., 2004).

15

16 Figure 9 shows comparisons between MOPITT retrievals and the MOZAIC-IAGOS climatology  
17 for global CO data at pressure levels 900 hPa, 700 hPa, 500 hPa, and 300 hPa. The biases and  
18 correlations between MOPITT CO VMR and the CO climatology (after applying the averaging  
19 kernels and the a priori profiles) are indicated in each plot. There are clearly two distinct clusters  
20 of dots in Fig. 9a and 9b, and the high CO VMR values seen here are from the tropics, with a  
21 very small number from the NH extratropics. Recent work by Ding et al. (2015) shows the  
22 association of enhanced CO in the free troposphere with the uplifting of CO from biomass  
23 burning and anthropogenic sources.

24 MOPITT and trajectory-mapped MOZAIC-IAGOS CO climatology mixing ratios are well-  
25 correlated with correlation coefficients of 0.7 or higher, for daytime data over both land and  
26 ocean. However, Fig. 9 also reveals significant biases between MOPITT retrievals and the  
27 trajectory-mapped MOZAIC-IAGOS CO climatology (geometric) altitudes above the 700 hPa  
28 pressure level. Although in Fig. 9 we have chosen to show biases for winter 2001-2012, the same  
29 analysis for other seasons yields similar results.

30

31

32 **Fig. 9.** Comparison results for DJF (December, January, February) 2001-2012. MOPITT CO  
33 retrievals at 900, 700, 500 and 300 hPa are plotted against trajectory-mapped MOZAIC-IAGOS  
34 CO climatology profiles that have been transformed using the MOPITT averaging kernels and a  
35 priori data. The red line is the 1:1 line,  $N$  denotes the total number of data points,  $R$  is the  
36 correlation coefficient,  $RMS$  is root mean square error in ppbv and  $Bias$  is the relative bias

1 between them in %. In each panel, the different color dots group different latitude bands: 23.5-  
2 66.5° S (SH extratropics), 23.5° S - 23.5° N (tropics) and 23.5-66.5° N (NH extratropics). .

3 These large differences are surprising, since Deeter et al. (2014), who also use the MOPITT L3  
4 V6 product and NOAA flask data (among other sources), report biases varying from -5.2% at  
5 400 hPa to 8.9% at the surface. These results are not dissimilar to our comparison in Figure 8,  
6 and would suggest a difference of about 5% between MOPITT and the trajectory-mapped  
7 climatology, with the climatology being higher primarily due to the airport effect. Although the  
8 validation data sets are not identical (owing primarily to incomplete global coverage of the  
9 MOZAIC-IAGOS product), the relative bias of 22% at 500 hPa seems excessive. In order to  
10 eliminate the possibility that trajectory errors might be contributing to [this](#) bias, we have also  
11 compared MOZAIC-IAGOS in situ CO profiles against MOPITT retrievals. As an example in  
12 Fig. 10, we display the comparison between MOZAIC-IAGOS in situ CO profiles at Frankfurt  
13 (Germany) and MOPITT CO retrievals, which have been regridded to 5° resolution, over  
14 Frankfurt from MOPITT overpasses. The MOZAIC-IAGOS in situ aircraft CO values have been  
15 transformed using the MOPITT averaging kernels and a priori data, for the period from  
16 December 2001- December 2012. MOPITT and MOZAIC-IAGOS are again strongly correlated,  
17 and biases at 500 hPa and 300 hPa are large, and in fact very similar in magnitude to those with  
18 respect to the trajectory-mapped MOZAIC-IAGOS CO dataset. This implies that the differences  
19 at 500 and 300 hPa are not a result of the trajectory mapping.

20

21

22 **Fig. 10.** Same as Fig. 9 but MOPITT CO retrievals are plotted against MOZAIC-IAGOS CO in  
23 situ profiles that have been transformed using the MOPITT averaging kernels and a priori data.  
24 The in situ profiles are monthly means from 2001-2012 (Frankfurt, Germany). Outliers (CO  
25 mixing ratios more than 1.5 standard deviations from the mean at each pressure level) have been  
26 removed, which improves the correlation coefficient at 300 hPa but makes no significant change  
27 in other derived parameters.

28 A global comparison between the trajectory-mapped MOZAIC-IAGOS climatology and  
29 MOPITT at 600 hPa is displayed in Fig. 11. As can be seen, both datasets capture major features  
30 of the CO distribution, particularly anthropogenically polluted (i.e., northeast China) and  
31 biomass burning (i.e., west Africa, central Africa, South Africa and central America) regions.  
32 The CO-rich air in the lower troposphere over west Africa, where biomass burning fires are  
33 active, is convectively lifted to the upper troposphere where it disperses over the African tropics  
34 towards the east coast of South America (Edwards et al., 2003). Over southern Africa and  
35 southeast Asia, where there are strong sources, and in general at 600 hPa, higher CO VMRs are  
36 found by the MOZAIC-IAGOS mapping than by MOPITT.

37

1

2 **Fig. 11.** Global distribution of the seasonal mean trajectory-mapped MOZAIC-IAGOS CO  
3 climatology (left panels), after transformation with the MOPITT a priori profiles and averaging  
4 kernels matrix, and MOPITT CO retrievals (right panels). CO mixing ratio (ppbv) as a function  
5 of latitude and longitude at 800 (a-d) and 600 (e-h) hPa pressure levels. Data are binned at  $5^\circ \times 5^\circ$   
6 in latitude and longitude for the period from 2001-2012.

7 Figure S2 shows global maps of percentage differences between MOPITT and the transformed  
8 trajectory-mapped MOZAIC-IAGOS CO climatology at 800 and 600 hPa pressure levels for DJF  
9 and SON 2001-2012. Differences are generally less than  $\pm 20\%$  at 800 hPa, with a negligible  
10 overall bias, but larger at 600 hPa, with MOPITT on average 10-20% lower. Generally, the  
11 comparisons of the CO profiles of the transformed trajectory-mapped MOZAIC-IAGOS and  
12 MOPITT for both grid cells as well as zonal mean for different latitude bands show a consistent,  
13 significant bias: MOPITT is lower from about 700 hPa to 300 hPa, but shows a negligible bias in  
14 the lowermost troposphere. Above 300 hPa, they seem to agree better, although this may be  
15 partly due to the fact that the retrieved CO values in this region are highly influenced by the  
16 MOPITT a priori data for both cases.

#### 17 4.2 Comparison with MOPITT CO total column values

18 In the same manner as we have done for the retrieved CO profiles, the retrievals of CO total  
19 column  $c_{ret}$  may be compared against total column values derived from in situ profiles  $x$ .  
20 Utilizing Eq. (2), the retrievals of the total CO column  $c_{ret}$  found in Eq. (3) can be rewritten  
21 alternatively as

$$22 \quad c_{ret} = c_a + \alpha(x - x_a) \quad (6)$$

23 where  $c_a = t^T x_a$  is the a priori total column value corresponding to the a priori profile  $x_a$ ,  $\alpha$   
24 is the CO total column averaging kernel and  $x$  is the in situ profile.

25 We have calculated the global total CO columns for both the MOZAIC-IAGOS CO climatology  
26 (using the MOPITT a priori and averaging kernels by applying Eq. (6)) and for MOPITT CO  
27 retrievals and compared different regions of the globe and different time intervals from 2001-  
28 2012. For most regions the MOPITT CO total columns are 10-20% lower than the trajectory-  
29 mapped MOZAIC-IAGOS CO climatology total columns, with larger differences in high CO  
30 source regions. The SH shows a distinct latitude gradient, which is not evident in the NH. This  
31 is likely related to the existence of major CO sources in the NH and the absence of large sources  
32 of emission in the SH. Figure 12 shows global total column CO for four seasons. It is clear that  
33 MOPITT and the climatology are similarly able to capture the CO spatial variability. In NH  
34 autumn, elevated total column CO is seen over South America, southeast Asia and west African  
35 which is due primarily to agricultural biomass burning in the regions. High total column CO is  
36 seen in all seasons over eastern China, which is one of the major emission regions in the world.



1 Northern hemispheric total columns are much higher than those in the southern hemisphere, and  
2 CO is somewhat more abundant in the NH winter, which is expected due to the lower amounts of  
3 hydroxyl radical (OH) that are present in the troposphere in that season. Difference plots for the  
4 CO maps shown Fig. 12 are shown in Figure S3.

5

6

7 **Fig. 12.** Global total column CO from the transformed trajectory-mapped MOZAIC-IAGOS  
8 climatology and MOPITT data for December-February, March-May, June-August and  
9 September-November 2001-2012. Data are averaged in  $5^{\circ}\times 5^{\circ}$  latitude- longitude bins.

10 Fig. 13 shows scatter plots of retrieved MOPITT CO total columns against the transformed  
11 trajectory-mapped MOZAIC-IAGOS climatology for the same periods shown in Fig. 12.  
12 Correlations are strong except in SON 2001-2012, and average biases 12-16%, with the  
13 trajectory MOZAIC-IAGOS higher. The high bias might be in part associated with the airport  
14 effect; however the averaging kernels (Fig. 3) are not very sensitive to CO in the boundary layer.

15

16

17 **Fig. 13.** Global MOPITT CO column retrievals versus transformed trajectory-mapped MOZAIC-  
18 IAGOS CO climatology column for four seasons. The bias is calculated as the difference for  
19 each grid cell,  $[2(MOPITT-Clim)/(Clim+MOPITT)]$ , averaged over all grid cells. The blue line is  
20 the line of best fit, the red line is the 1:1 line and the correlation coefficient ( $R$ ), total number of  
21 data points ( $N$ ) and root mean square error (RMS) are indicated.

## 22 **5 Results**

### 23 **5.1 Global distribution of MOZAIC-IAGOS CO climatology**

24 Figure 14 shows the monthly mean CO VMR between 4 and 8 km altitude above sea level for  
25 2001-2012. The climatology is able to capture the CO spatial variability fairly well: the northern  
26 hemispheric concentrations are much higher, and the biomass burning peaks are clearly visible  
27 for the NH winter and spring seasons. The climatology shows more abundant CO in the NH  
28 during these seasons. This is due primarily to lower OH levels during the cold season which  
29 permits a longer lifetime for CO, although there also appears to be an additional source in eastern  
30 Asia. Enhanced CO concentration is observed in the tropical regions where wildfire burning is  
31 typical during January–April, like west Africa and a large part of central Africa (Sauvage et al.,  
32 2005, 2007). At southern mid-latitudes between South America, southern Africa and Australia,  
33 we observe high CO from September to November, during the agricultural burning season.  
34 Although Fig. 14 shows a 12-year global map, the strong enhanced CO over these regions (west

1 Africa, South America, and southeast Asia) is clearly observable as an annual feature with  
2 significant interannual variability.

3

4

5

6 **Fig. 14.** Global monthly mean CO distribution from the trajectory-mapped MOZAIC-IAGOS  
7 CO VMR as a function of latitude and longitude for January-December 2001-2012 and altitudes  
8 between 4-8 km a.s.l. The data are averaged with a bin size of  $5^{\circ} \times 5^{\circ}$ .

## 9 **5.2 Zonal distribution of MOZAIC-IAGOS CO climatology**

### 10 **5.2.1 Seasonal variation**

11

12 **Fig. 15.** Zonally averaged monthly variation of CO for the latitude bands  $45^{\circ}\text{S}$ - $45^{\circ}\text{N}$ ,  $23.5^{\circ}\text{S}$ -  
13  $23.5^{\circ}\text{N}$ ,  $23.5$ - $66.5^{\circ}\text{N}$  and  $23.5$ - $66.5^{\circ}\text{S}$ , for the period 2001-2012. CO mixing ratios are shown for  
14 altitude ranges 0-2 km, 2-4 km, 4-8 km and 8-12 km, as well as total column (TC).

15 As can be seen from Fig. 15, CO shows distinct seasonal cycles in both hemispheres. In the NH  
16 extratropics (Fig. 15c), maximum CO VMR is observed in February-April following a steady  
17 increase during fall and winter. This is followed by a rapid decrease to the lowest CO levels in  
18 July-September. The decline in summer shows the typical seasonal pattern of CO in the NH  
19 driven by OH increase during this time (Yurganov et al., 2008; Novelli et al., 1998). In the SH  
20 extratropics (Fig. 15d), CO levels peak in September-October. This is consistent with previous  
21 studies by Novelli et al. (1998). In the SH, the annual CO maximum is earlier at lower altitudes.  
22 Rinsland et al. (2002) suggested this phenomenon to be associated with the vertical and  
23 horizontal CO dispersion away from the biomass burning region in the tropics. Moreover, CO  
24 shows greater seasonal variability, particularly at higher altitudes, in the SH than in the NH. The  
25 seasonal CO cycle in the tropics (Fig. 15b) and for latitude band  $45^{\circ}\text{S}$ - $45^{\circ}\text{N}$  (Fig. 15a) both  
26 display a July minimum, and a secondary maximum in October while the primary maximum is in  
27 late NH winter/early spring. The CO cycle in both hemispheres is controlled by seasonal  
28 variations of OH (Logan et al., 1981; Bergamaschi et al., 2000; Novelli et al., 1998) and biomass  
29 burning in the tropics and to a lesser degree at boreal latitudes.

30 Figure 16 shows zonal mean latitude-time cross-section plots of CO VMR at 2.5 km, 4.5 km, 6.5  
31 km, 8.5 km, 10.5 km and 12.5 km altitudes for the period 2001-2012. The latitude-time cross-  
32 section shows the seasonal cycle of zonal mean CO for different altitudes, as seen in the previous  
33 figures, and also the variation of the interhemispheric CO VMR gradient throughout the year.  
34 The strongest interhemispheric gradient occurs in March, at low altitude, and the smallest

1 gradients are seen in northern summer. The gradient in NH spring reverses at higher altitudes,  
2 and in NH fall where it is especially strong at higher altitudes. Plots 14e, f also clearly show the  
3 weak seasonal cycle in the NH upper troposphere compared to that in the SH.

4

5

6

7 **Fig. 16.** Seasonal variation of zonal monthly mean trajectory-mapped MOZAIC-IAGOS CO  
8 climatology at 2.5 , 4.5, 6.5, 8.5, 10.5 and 12.5 km altitudes for the period 2001-2012. The zonal  
9 mean data are averaged in 5° latitude intervals.

### 10 **5.3.2 Vertical distribution**

11 Figure 17 illustrates the variation of CO with altitude for the seasons in which we observe  
12 maximum CO levels in both the SH and NH (i.e., MAM and SON). The greatest CO VMRs are  
13 found at lower altitudes in both hemispheres, although CO declines with altitude faster in the NH  
14 than the SH. This results in a decrease in the strength of the interhemispheric gradient (SH to  
15 NH) with altitude. This result is consistent with Edwards et al. (2006) who suggested that in the  
16 absence of continued CO input from the source regions (i.e., biomass burning in southern Africa  
17 and South America), the aged CO is gradually distributed vertically throughout the troposphere  
18 in the SH. In fact, in regions where there is deep convection this leads to an enhanced CO  
19 concentration in the upper troposphere, as can be seen on the right-hand side of Fig. 17 and in  
20 Fig. 18. Moreover, Liu et al. (2006) showed large horizontal CO gradients in association with  
21 vertical and horizontal transport of air with different chemical signatures of origin.

22 Zonal CO mean vertical profiles for February, April, July and September, averaged for 2001-  
23 2012 over the latitude bands 23.5-66.5° N (NH extratropics), 23.5-66.5° S (SH extratropics) and  
24 23.5° S-23.5° N (tropics), are shown in Fig. 18. The CO profiles show seasonal and latitudinal  
25 variability primarily in the NH extratropics. The largest VMRs of CO occur at lower altitudes in  
26 the NH extratropics in February and April but the strong decline with altitude causes CO VMRs  
27 to be higher in the SH at high altitudes than in the NH. The trajectory-mapped CO in the SH  
28 extratropics is mainly representative of the tropics, while in the NH extratropics there are many  
29 CO measurements poleward of 40°. This implies that sampling of the lowermost stratosphere  
30 will be more frequent in the NH than in the SH. In the tropics, CO VMRs show a rapid decrease  
31 with altitude in the lower troposphere but above approximately 4-5 km changes with altitude are  
32 minor.

33

34

35

1 **Fig. 17.** Global distribution of seasonal (the NH spring and fall) mean trajectory-mapped  
2 MOZAIC-IAGOS CO climatology as a function of latitude and longitude for altitudes 1.5, 3.5,  
3 5.5 km, 7.5 km and 9.5 km a.s.l. The left and right columns show average CO VMRs for March-  
4 April-May and September-October-November, 2001-2012. The data are averaged with a bin size  
5 of  $5^{\circ} \times 5^{\circ}$  latitude and longitude.

6

7

8 **Fig. 18.** Monthly mean profiles of CO from the trajectory-mapped MOZAIC-IAGOS CO  
9 climatology for February, April, July and September, averaged for 2001-2012. The different  
10 colors represent CO mean VMR for the latitude bands  $23.5\text{-}66.5^{\circ}\text{N}$ ,  $23.5\text{-}66.5^{\circ}\text{S}$  and  $23.5^{\circ}\text{S-}$   
11  $23.5^{\circ}\text{N}$ .

## 12 **6 Applications**

### 13 **6.1 Global variation and trends of CO**

14 The smoothed time series of the NH extratropical zonal mean CO VMR at 900, 700, 500, and  
15 300 hPa for the trajectory-mapped MOZAIC-IAGOS dataset 2001-2012 is shown in Fig. 19. For  
16 purposes of comparison we also show data from MOPITT and from the mapped MOZAIC-  
17 IAGOS dataset transformed with the MOPITT averaging kernels. Gaps in the figure occur  
18 whenever one data source is missing. The gaps in June-July 2001 and August-September 2009  
19 were due to a cooler failure of the MOPITT instrument. MOZAIC-IAGOS began CO  
20 measurement in December 2001 and there were only partial data available in 2010 and 2011. The  
21 observations show an annual late winter or springtime peak in the NH extratropical zonal CO  
22 loading each year, in conjunction with low wintertime OH levels. The same interannual cycle of  
23 CO is captured by both trajectory-mapped MOZAIC-IAGOS (transformed and untransformed)  
24 and MOPITT. They appear to track short-term changes equally well. However, while all show a  
25 modest decline in the lower troposphere until about 2008-2009 (after which CO VMR seems to  
26 level off), in accordance with the trends found by Worden et al. (2013), in the upper troposphere  
27 MOPITT shows a modest increase. It also shows a significant bias with respect to the trajectory-  
28 mapped MOZAIC-IAGOS data that decreases with time. Although the untransformed trajectory-  
29 mapped MOZAIC-IAGOS CO values show a significant difference against the transformed data  
30 in the lower troposphere, they seem to agree well at higher levels. The untransformed trajectory-  
31 mapped MOZAIC-IAGOS data show higher CO levels than MOPITT CO retrievals at all levels.

32

33

34 **Fig. 19.** Zonally averaged time series of monthly mean CO VMR, at individual levels and total  
35 column, as retrieved by MOPITT and from the trajectory-mapped MOZAIC-IAGOS CO

1 climatology (untransformed, and transformed using MOPITT's averaging kernels) for the  
2 latitude band 23.5°-66.5° N.

3 Laken and Shahbaz (2014) found increasing CO trends over widespread regions of South  
4 America, Mexico, central Africa, Greenland, the eastern Antarctic, and the entire region of India  
5 and China from MOPITT data. The SH extratropics also shows time series similar to those in  
6 Fig. 19, but the negative trend is not as clear as that in the NH due to limited data. The annual  
7 springtime peak in the SH zonal CO loading is visible in all of the time series. This is  
8 predominantly associated with dry season biomass burning emissions in South America,  
9 southern Africa, southeast Asia, and northwestern Australia. In later months, the CO resulting  
10 from these emissions is generally destroyed by more active photochemistry during the SH  
11 summer. At these times, the retrieved zonal CO falls to background levels (around 40-50 ppbv)  
12 which are representative of the remote ocean regions where CO production by methane oxidation  
13 is the dominant source (Edwards et al., 2006). We looked at the time series of the zonal monthly  
14 mean of CO VMR for the tropics. The biases between the MOPITT retrievals and the trajectory-  
15 mapped MOZAIC-IAGOS in general show the same features as for the extratropics, while the  
16 seasonal patterns combine those of the NH and SH seen in Fig. 19.

17 In Fig. S4, we display the monthly mean time series for Frankfurt from December 2001-  
18 December 2012. These also show significant biases, declining with time, between MOPITT and  
19 the transformed MOZAIC-IAGOS in situ above 700 hPa, in good agreement with the result  
20 shown in Fig. 19. Furthermore, MOPITT shows a modest increase in CO levels in the upper  
21 troposphere while MOZAIC-IAGOS in situ (transformed and untransformed) shows a modest  
22 decline, consistent with Petetin et al. (2015), who report a similar decrease over Frankfurt. The  
23 MOPITT and MOZAIC-IAGOS (transformed and untransformed) CO values for Frankfurt show  
24 the same seasonal patterns as the NH extratropics (Fig. 19). This comparison suggests that a  
25 prominent bias, declining with time, exists between MOZAIC-IAGOS and MOPITT L3 V6  
26 TIR/NIR products.

27

28

## 29 **7 Conclusions**

30 We have presented a three-dimensional (i.e., latitude, longitude, altitude) gridded climatology of  
31 CO developed by trajectory mapping of global MOZAIC-IAGOS data. This quasi-global  
32 climatology dataset offers a complement to global satellite measurements, at significantly higher  
33 vertical resolution, that facilitates visualization and comparison of different years and seasons,  
34 and offers insight into the global variation and trends of CO. Even though the MOZAIC-IAGOS  
35 aircraft data are unevenly distributed both in time and space across the globe, the trajectory-  
36 mapped dataset is uniformly distributed on a 5°×5°×1 km grid. Major regional features of the

1 global CO distribution are clearly evident in the CO maps for different seasons and altitudes. The  
2 trajectory-mapped CO shows distinct seasonal cycles with the CO annual maximum occurring in  
3 September-October in the SH, coincident with the tropical biomass burning season (Rinsland et  
4 al., 2002), and in April in the NH, while the tropics show distinct maxima in January-February  
5 and in October. We caution that the observed result in the SH is obtained from the limited data  
6 we have from the region. The interhemispheric CO gradient is strongest in late winter/early  
7 spring, and smallest in northern summer. Time series analysis of the climatology shows that in  
8 the NH and the tropics CO is declining with time. This is consistent with previous studies using  
9 ground-based, aircraft and satellite data, such as Petetin et al. (2015), Worden et al. (2013),  
10 Laken and Shahbaz (2014) and Novelli et al. (1998). The consistency of our findings with those  
11 from other global datasets lends increased confidence that the CO dataset derived from trajectory  
12 mapping of global MOZAIC-IAGOS data can be used for CO trend studies at regional and  
13 global scales.

14 The trajectory-mapped CO dataset has been validated by comparing maps constructed using only  
15 forward trajectories and using only backward trajectories. The two methods show similar global  
16 CO distribution patterns. Differences are most commonly 10% or less, and found to be less than  
17 30% for almost all cases. They are typically less than 10% at northern mid-latitudes and less than  
18 20% in the tropics between  $\pm 30^\circ$  latitude, except in the Pacific and Atlantic oceans where it can  
19 reach as large as 30%. The dataset has also been validated by comparison against in-situ  
20 MOZAIC-IAGOS aircraft measurements, where the data from the validation site are excluded  
21 from the trajectory-mapped data. Although the comparison shows larger differences below 2 km,  
22 the profiles from the two methods agree very well between 2 and 10 km with the magnitude of  
23 differences within 20%. A further comparison between the trajectory-mapped result and  
24 MOZAIC-IAGOS in situ CO cruise data, which were not included in the trajectory-mapping,  
25 shows that major regional features of the global CO distribution for different seasons are clearly  
26 evident in both maps and they agree well in regions of overlap. This suggests that the trajectory-  
27 mapped CO data performs well not only near airports but also in remote areas. Validation was  
28 also performed against independent data from the NOAA aircraft flask sampling program. The  
29 results suggest small or insignificant biases in the upper troposphere, but positive biases as large  
30 as 12% for MOZAIC-IAGOS in the lower troposphere. This is probably due to the “airport  
31 effect”, a sampling bias that occurs because commercial aircraft operate from large airports near  
32 large cities, with typically elevated CO levels in the boundary layer.

33 The trajectory-mapped CO dataset has also been extensively compared with MOPITT retrievals.  
34 Between 700 and 300 hPa, a prominent bias, declining with time, exists between MOZAIC-  
35 IAGOS and MOPITT L3 V6 TIR/NIR products.

36

37 This study demonstrates one aspect of the value of the MOZAIC-IAGOS continuous, long-term,  
38 global, vertically resolved in situ measurements. Such routine commercial aircraft observations

1 provide valuable information on atmospheric composition that can improve our understanding of  
2 global and regional air quality and the potential impact of greenhouse gases on climate change.  
3 [The dataset](#) The unique 3D CO climatology dataset presented here has the potential to be used  
4 for time series and trend analysis, and provides a quasi-global view of CO changes and transport  
5 as well as interannual variability. It will also be useful as model initial fields, and background  
6 and boundary fields. It will be especially useful as an improved a priori climatology for satellite  
7 data retrieval. The global picture it presents is also expected to be valuable for comparison and  
8 validation of model results. The data are publically available at [ftp://es-  
9 ee.tor.ec.gc.ca/pub/ftpd/MOZAIC\\_output\\_CO/](ftp://es-ee.tor.ec.gc.ca/pub/ftpd/MOZAIC_output_CO/).

10

11 **Acknowledgements.** The authors acknowledge the strong support of the European Commission,  
12 Airbus, and the Airlines (Lufthansa, Air-France, Austrian, Air Namibia, Cathay Pacific, Iberia  
13 and China Airlines so far) who carry the MOZAIC or IAGOS equipment and perform the  
14 maintenance since 1994. MOZAIC is presently funded by INSU-CNRS (France), Météo-France,  
15 Université Paul Sabatier (Toulouse, France) and Research Center Jülich (FZJ, Jülich, Germany).  
16 IAGOS has been additionally funded by the EU projects IAGOS-DS and IAGOS-ERI. The  
17 MOZAIC-IAGOS database is supported by ETHER (CNES and INSU-CNRS). Data are also  
18 available via Ether web site <http://www.pole-ether.fr>. We thank the many whose dedication  
19 makes such a dataset possible. The MOPITT data were obtained from the NASA Langley  
20 Research Center Atmospheric Science Data Center. We thank R. Draxler and the NOAA Air  
21 Resources Laboratory for the trajectory model HYSPLIT, and NCEP/NCAR for the global  
22 meteorological reanalysis data. The first author is grateful to the Natural Sciences and  
23 Engineering Research Council of Canada (NSERC) and Environment Canada for a research  
24 fellowship. Important discussions with Merritt Deeter regarding MOPITT averaging kernels are  
25 much appreciated. We thank Paul Novelli and Colm Sweeney of NOAA/[Earth System Research  
26 Laboratory Global Monitoring Division](#) and Steven Wofsy of Harvard University/School of  
27 Engineering and Applied Sciences for providing the in situ CO profiles.

## 28 **References**

29 | Bergamaschi, P., R. Hein, M. Heimann, and P. J. Crutzen, Inverse modeling of the global CO  
30 cycle: 1. Inversion of CO mixing ratios, *J. Geophys. Res.*, 105(D2), 1909  
31 doi:10.1029/1999JD900818, 2000.

32 | Boden, T. A., G. Marland, and R. J. Andres, Global, Regional, and National Fossil-Fuel CO<sub>2</sub>  
33 Emissions. Carbon Dioxide Information Analysis Center, Oak Ridge Natl. Lab., U.S. Dep. of  
34 Energy, Oak Ridge, Tenn., doi:10.3334/CDIAC/00001. (Available at  
35 <http://cdiac.ornl.gov/trends/emis/cpa.html>), (last access: 8 September 2015), 2009.

Formatted: Left

- 1 | Brook, J.R., T.F. Dann, E. Galarneau, D. Herod and J.-P. Charland, (2014), The State of Air  
2 | Quality in Canada: National Patterns, in *Air Quality Management, Canadian Perspectives on a*  
3 | *Global Issue*, Springer, Dordrecht, ISBN 978-94-007-7557-2, 43-67, doi: 10.1007/978-94-007-  
4 | 7557-2
- 5 | Cai, H., and S. Xie, Estimation of vehicular emission inventories in China from 1980 to 2005,  
6 | *Atmos. Environ.*, 44(39), 8963–8979, 2007.
- 7 | Carmichael, G. R., Y. Tang, G. Kurata, I. Uno, D.G. Streets, J-H Woo, H. Huang, J. Yienger, B.  
8 | Lefer, R.E. Shetter, D.R. Blake, E. Atlas, A. Fried, E. Apel, F. Eisele, C. Cantrell, M.A. Avery,  
9 | J.D. Barrick, G.W. Sachse, W.L. Brune, S.T. Sandholm, Y. Kondo, H.B. Singh, R.W. Talbot, A.  
10 | Bandy, D. Thornton, A.D. Clarke, and B.G. Heikes, Regional-scale chemical transport modeling  
11 | in support of intensive field experiments: Overview and analysis of the TRACE-P observations,  
12 | *J. Geophys. Res.*, 108(D21), 8823, doi:10.1029/2002JD003117, 2003.
- 13 | Chameides, W., ~~L.~~, P.S. Kasibhatla, J. J. Yienger, H. Levy II, and W. J. Moxim, The growth  
14 | of continental-scale metro-agro-plexes, regional ozone pollution, and world food production,  
15 | *Science*, 264, 74-77, 1994.
- 16 | Clark H., B. Sauvage, V. Thouret, P. Nédélec, R. Blot, K.Y. Wang, H. Smit, P. Neis, A. Petzold,  
17 | G. Athier, D. Boulanger, J-M. Cousin, K. Beswick, M. Gallagher, D. Baumgardner, J. Kaiser, J-  
18 | M. Flaud, A. Wahner, A. Volz-Thomas and J-P. Cammas, The first regular measurements of  
19 | ozone, carbon monoxide and water vapour in the Pacific UTLS by IAGOS, *Tellus B*, 67, 28385,  
20 | <http://dx.doi.org/10.3402/tellusb.v67.28385>, 2015.
- 21 | Conway, T. J., P. P. Tans, L. S. Waterman K., W. Thoning D., R. Kitzis, K. A. Masarie, and N  
22 | . Zhang, Evidence for interannual variability of the carbon cycle from the NOAA/CMDL global  
23 | air sampling network, *J. Geophys. Res.*, 99, 22,831-22,855, 1994.
- 24 | Crutzen, P. A., A discussion of the chemistry of some minor constituents in the stratosphere and  
25 | troposphere, *Pure and Applied Geophysics* 106-108, 1385-1399, doi:  
26 | [10.1007/BF00881092](http://dx.doi.org/10.1007/BF00881092), 1973.
- 27 | Deeter, M. N. (2002), Calculation and Application of MOPITT (Measurements of Pollution in  
28 | the Troposphere) Averaging Kernels, Available at  
29 | [http://www.acom.ucar.edu/mopitt/data/avg\\_krnls\\_app.pdf](http://www.acom.ucar.edu/mopitt/data/avg_krnls_app.pdf)
- 30 | Deeter, M. N., L. K. Emmons, D. P. Edwards, J. C. Gille, and J. R. Drummond, Vertical  
31 | resolution and information content of CO profiles retrieved by MOPITT, *Geophys. Res. Lett.*,  
32 | 31, L15112, doi:10.1029/2004GL020235, 2004.

Formatted: Left, Don't adjust space between Latin and Asian text

Formatted: Left



- 1 | Deeter, M. N., MOPITT (Measurements of Pollution in the Troposphere) Validated Version 5  
2 | Product User's Guide, National Center for Atmospheric Research. Available at  
3 | [http://www.acom.ucar.edu/mopitt/v5\\_users\\_guide\\_beta.pdf](http://www.acom.ucar.edu/mopitt/v5_users_guide_beta.pdf), 2011.
- 4 | Deeter, M., H.M. Worden, D.P. Edwards, J.C. Gille, and A.E. Andrews: Evaluation of MOPITT  
5 | retrievals of lower-tropospheric carbon monoxide over the United States, *J. Geophys. Res.*, 117,  
6 | D13306, DOI: 10.1029/2012JD017553, 2012.
- 7 | Deeter, M. N., Edwards, D. P., Gille, J. C., Emmons, L. K., Francis, G., Ho, S.-P., Mao, D.,  
8 | Masters, D., Worden, H., Drummond, J. R., and Novelli, P.: The MOPITT Version 4 CO  
9 | Product: Algorithm Enhancements, Validation, and Long-Term Stability, *J. Geophys. Res.*, 115,  
10 | D07306, doi:10.1029/2009JD013005, 2010.
- 11 | Deeter, M. N., Martínez-Alonso, S., Edwards, D. P., Emmons, L. K., Gille, J. C., Worden, H. M.,  
12 | Pittman, J. V., Daube, B. C., and Wofsy, S. C.: Validation of MOPITT Version 5 thermal-  
13 | infrared, near-infrared, and multispectral carbon monoxide profile retrievals for 2000–2011, *J.*  
14 | *Geophys. Res.*, 118, 6710–6725, doi:10.1002/jgrd.50272, 2013.
- 15 | Deeter, M. N., Martínez-Alonso, S., Edwards, D. P., Emmons, L. K., Gille, J. C., Worden, H. M.,  
16 | Sweeney, C., Pittman, J. V., Daube, B. C., and Wofsy, S. C.: The MOPITT Version 6 product:  
17 | algorithm enhancements and validation, *Atmos. Meas. Tech.*, 7, 3623-3632, 2014.
- 18 | Ding, K., Liu, J., Ding, A., Liu, Q., Zhao, T. L., Shi, J., Han, Y., Wang, H., Jiang, F.:  
19 | Uplifting of carbon monoxide from biomass burning and anthropogenic sources to the free  
20 | troposphere in East Asia, *Atmos. Chem. Phys.* 15, 2843-2866, doi:10.5194/acp-15-2843-2015,  
21 | 2015.
- 22 | Draxler, R. R.: HYSPLIT4 user's guide, NOAA Tech. Memo, ERL ARL-230, NOAA Air  
23 | Resources Laboratory, Silver Spring, MD, 1999.
- 24 | Draxler, R.R., Hess, G.D., An overview of the Hysplit\_4 modeling system for trajectories,  
25 | dispersion, and deposition. *Australian Meteorological Magazine* 47, 295–308, 1998.
- 26 | Drummond, J. R., and G. S. Mand, The Measurements of Pollution in the Troposphere  
27 | (MOPITT) instrument: Overall performance and calibration requirements, *J. Atmos. Oceanic*  
28 | *Technol.*, 13, 314–320, 1996.
- 29 | Edwards, D. P., Lamarque, J.-F., Attie', J.-L., Emmons, L. K., Richter, A., Cammas, J.-P.,  
30 | Gille, J. C., Francis, G. L., Deeter, M. N., Warner, J., Ziskin, D. C., Lyjak, L. V., Drummond, J.  
31 | R., and Burrows, J. P.: Tropospheric ozone over the tropical Atlantic: A satellite perspective, *J.*  
32 | *Geophys. Res.*, 108(D8), 4237, doi:10.1029/2002JD002927, 2003.

- 1 | Edwards, D. P., C. Halvorson, and J. C. Gille, Radiative transfer modeling of the EOS Terra  
2 | Satellite Measurements of Pollution in the Troposphere (MOPITT) instrument, *J. Geophys. Res.*,  
3 | 104, 16,755–16,775, 1999.
- 4 | Edwards, D. P., G. Petron, P. C. Novelli, L. K. Emmons, J. C. Gille, and J. R. Drummond,  
5 | Southern Hemisphere carbon monoxide interannual variability observed by Terra/Measurement  
6 | of Pollution in the Troposphere (MOPITT), *J. Geophys. Res.*, 111, D16303,  
7 | doi:10.1029/2006JD007079, 2006.
- 8 | Emmons, L. K., D. P. Edwards, M. N. Deeter, J. C. Gille, T. Campos, P. Nedelec, P. Novelli,  
9 | and G. Sachse, Measurements of Pollution In The Troposphere (MOPITT) validation through  
10 | 2006, *Atmos. Chem. Phys.*, 9, 1795–1803, 2009.
- 11 | Emmons, L. K., G. G. Pfister, D. P. Edwards, J. C. Gille, G. Sachse, D. Blake, S. Wofsy, C.  
12 | Gerbig, D. Matross, and P. ~~Ne´de´lec~~[Nédélec](#), Measurements of Pollution in the Troposphere  
13 | (MOPITT) validation exercises during summer 2004 field campaigns over North America, *J.*  
14 | *Geophys. Res.*, 112, D12S02, doi:10.1029/2006JD007833, 2007.
- 15 | Emmons, L. K., Gille, J. C., Edwards, D. P., Attie´, J.-L., Warner, J., Ziskin, D., Francis, G.,  
16 | Khattatov, B., Yudin, V., Lamarque, J.-F., Ho, S.-P., Mao, D., Chen, J. S., Drummond, J.,  
17 | Novelli, P., Sachse, G., Coffey, M. T., Hannigan, J. W., Gerbig, C., Kawakami, S., Kondo,  
18 | Y., Takegawa, N., Schlager, H., Baehr, J., Ziereis, H., Validation of Measurements of Pollution  
19 | in the Troposphere (MOPITT) CO retrievals with aircraft in situ profiles, *J. Geophys. Res.*, 109,  
20 | D03309, doi:10.1029/2003JD004101, 2004.
- 21 | Fishman, J., and Seiler, W., Correlative Nature of Ozone and Carbon Monoxide in the  
22 | Troposphere: Implications for the Tropospheric Ozone Budget, *J. Geophys. Res.*, 88, C6, 3662-  
23 | 3670, 1983.
- 24 | Galanter, M., H. Levy II, and G. R. Carmichael, Impacts of biomass burning on tropospheric CO,  
25 | NOx, and Os, *J. Geophys. Res.*, 105, 6633-6653, 2000.
- 26 | Granier, C., Bessagnet, B., Bond, T., D’Angiola, A., v. d. Gon, H. D., Frost, G. J., Heil, A.,  
27 | Kaiser, J. W., Kinne, S., Klimont, Z., Kloster, S., Lamarque, J.-F., Liousse, C., Masui, T.,  
28 | Meleux, F., Mieville, A., Ohara, T., Raut, J.-C., Riahi, K., Schultz, M. G., Smith, S. J., Thomson,  
29 | A., v. Aardenne, J., v. d. Werf, G. R., and v. Vuuren, D. P.: Evolution of anthropogenic and  
30 | biomass burning emissions of air pollutants at global and regional scales during the 1980–2010  
31 | period, *Clim. Change*, 109, 163–190, doi:10.1007/s10584-011-0154-1, 2011.
- 32 | Gregg, J. S., R. J. Andres, and G. Marland, China: Emissions pattern of the world leader in CO2  
33 | emissions from fossil fuel consumption and cement production, *Geophys. Res. Lett.*, 35, L08806,  
34 | doi:10.1029/ 2007GL032887, 2008.

- 1 | Heald, C. L., Jacob, D. J., Jones, D. B. A., Palmer, P. I., Logan, J. A., Streets, D. G., Sachse, G.  
2 | W., Gille, J. C., Hoffman, R. N., and Nehrkorn, T.: Comparative inverse analysis of satellite  
3 | (MOPITT) and aircraft (TRACE-P) observations to estimate Asian sources of carbon monoxide,  
4 | *J. Geophys. Res.*, 109, D15S04, doi:10.1029/2004JD005185, 2004.
- 5 | Holloway, T., Levy II, H., Kasibhatla, P., Global distribution of carbon monoxide. *J. Geophys.*  
6 | *Res.*, 105, 12123e12147, 2000.
- 7 | Hoor, P., Gurk, C., Brunner, D., Hegglin, M. I., Wernli, H., and Fischer, H.: Seasonality and  
8 | extent of extratropical TST derived from in-situ CO measurements during SPURT, *Atmos.*  
9 | *Chem. Phys.*, 4, 1427–1442, 2004.
- 10 | Hubler, G., Montzka, D. D., Norton, R. B., Murphy, P. C., Fehsenfeld, F. C., Liu, S. C., Ridley,  
11 | B. A., Walega, J. G., Atlas, E., Grahek, F. E., Heidt, L. E., Merrill, J., Huebert, B. J., and  
12 | Bodhaine, B. A.: Total reactive oxidized nitrogen (NO<sub>y</sub>) in the remote pacific troposphere and  
13 | its correlation with O<sub>3</sub> and CO: Mauna Loa Observatory Photochemistry Experiment 1988, 25, *J.*  
14 | *Geophys. Res.*, 97, 10 427–10 447, 1992.
- 15 | IPCC, 2013 (IPCC AR5): Climate Change 2013: The Physical Science Basis. Contribution of  
16 | Working Group I to the Fifth Assessment Report of the Intergovernmental Panel on Climate  
17 | Change [Stocker, T.F., D. Qin, G.-K. Plattner, M. Tignor, S.K. Allen, J. Boschung, A. Nauels, Y.  
18 | Xia, V. Bex and P.M. Midgley (eds.)]. Cambridge University Press, Cambridge, United  
19 | Kingdom and New York, NY, USA, 1535 pp.
- 20 | Jacob, D. J., Crawford, J. H., Kleb, M. M., Connors, V. S., Bendura, R. J., Raper, J. L., Sachse,  
21 | G. W., Gille, J. C., Emmons, L., and Heald, C. L.: Transport and Chemical Evolution over the  
22 | Pacific (TRACE-P) aircraft mission: Design, execution, and first results, *J. Geophys. Res.*,  
23 | 108(D20), 9000, doi:10.1029/2002JD003276, 2003.
- 24 | Jaffe, D.A., R.E. Honrath, L. Zhang, H. Akimoto, A. Shimizu, H. Mukai, K. Murano, S.  
25 | Hatakeyama, and J. Merrill, Measurements of NO, NO<sub>y</sub>, CO, and O<sub>3</sub> and estimation of the  
26 | ozone production rate at Oki Island, Japan during PEM-West, *J. Geophys. Res.*, 101, 2037-2048,  
27 | 1996.
- 28 | Kalnay, E., Kanamitsu, M., Kistler, R., Collins, W., Deaven, D., Gandin, L., Iredell, M., Saha,  
29 | S., White, G., Woollen, J., Zhu, Y., Leetmaa, A., Reynolds, R., Chelliah, M., Ebisuzaki, W., 30  
30 | Higgins, W., Janowiak, J., Mo, K. C., Ropelewski, C., Wang, J., Jenne, R., and Joseph, D.: The  
31 | NCEP/NCAR 40-year reanalysis project, *B. Am. Meteorol. Soc.*, 77, 437–471, 1996.
- 32 | Khalil, M. A. K., and R. A. Rasmussen, Carbon monoxide in the Earth's atmosphere: Indications  
33 | of a global increase, *Nature*, 332, 242-245, 1988.
- 34 | Khalil, M. A. K., and R. A. Rasmussen, Global decrease in atmospheric carbon monoxide  
35 | concentration, *Nature*, 370, 639-641, 1994.

- 1 | Kim, P. S., D. J. Jacob, X. Liu, J. X. Warner, K. Yang, K. Chance, V. Thouret, and P. Nedelec,  
2 | Global ozone–CO correlations from OMI and AIRS: constraints on tropospheric ozone sources,  
3 | *Atmos. Chem. Phys.*, 13, 9321–9335, 2013.
- 4 | Laken, B., Shahbaz, T., Satellite-Detected Carbon Monoxide Pollution during 2000–2012:  
5 | Examining Global Trends and also Regional Anthropogenic Periods over China, the EU and the  
6 | USA, *Climate*, 2(1), 1-16; doi:10.3390/cli2010001, 2014.
- 7 | Lang, P.M., L. P. Steele, L. S. Waterman, R. C. Martin, K. A. Masarie, and E. J. Dlugokencky  
8 | NO AA/CMDL atmospheric methane data for the period 1983-1990 from shipboard flask  
9 | sampling NOAA Tech. Memo., ERL CMDL-4, 88 pp., 1992.
- 10 | Law, K. S., and J. A. Pyle, Modeling trace gas budgets in the troposphere 2. CH<sub>4</sub> and CO, *J.*  
11 | *Geophys. Res.*, 98, 18401–18412, doi:10.1029/93JD01480, 1993.
- 12 | Lelieveld, J., P. J. Crutzen, V. Ramanathan, M. O. Andreae, C. A. M. Brenninkmeijer, T.  
13 | Campos, G. R. Cass, R. R. Dickerson, H. Fischer, J. A. de Gouw, A. Hansel, A. Jefferson, D.  
14 | Kley, A. T. J. de Laat, S. Lal, M. G. Lawrence, J. M. Lobert, O. L. Mayol-Bracero, A. P. Mitra, T.  
15 | Novakov, S. J. Oltmans, K. A. Prather, T. Reiner, H. Rodhe, H. A. Scheeren, D. Sikka, J.  
16 | Williams, The Indian Ocean Experiment: Widespread air pollution from south and Southeast  
17 | Asia, *Science*, 291, 1031– 1036, 2001.
- 18 | Liu, G., D. W. Tarasick, V. E. Fioletov, C. E. Sioris, and Y. J. Rochon, Ozone correlation lengths  
19 | and measurement uncertainties from analysis of historical ozonesonde data in North America and  
20 | Europe, *J. Geophys. Res.*, 114, D04112, doi:10.1029/2008JD010576, 2009.
- 21 | Liu, G., J. Liu, D. W. Tarasick, V. E. Fioletov, J. Jin, O. Moeini, X. Liu, and C. E. Sioris, A  
22 | global tropospheric ozone climatology from trajectory-mapped ozone soundings, *Atmos. Chem.*  
23 | *Phys.* 13, 10659-10675, doi:10.5194/acp-13-10659-2013, 2013.
- 24 | Liu, H., D. J. Jacob, I. Bey, R. M. Yantosca, B. N. Duncan, and G. W. Sachse, Transport  
25 | pathways for Asian combustion outflow over the Pacific: Interannual and seasonal variations, *J.*  
26 | *Geophys. Res.*, 108(D20), 8786, doi:10.1029/2002JD003102, 2003.
- 27 | Liu, J., D. W. Tarasick, V. E. Fioletov, C. McLinden, T. Zhao, S. Gong, C. Sioris, J. J. Jin, G.  
28 | Liu, and O. Moeini, A global ozone climatology from ozone soundings via trajectory mapping: a  
29 | stratospheric perspective, *Atmos. Chem. Phys. Discuss.*, 13, 16831–16883, 2013.
- 30 | Liu, J., J. R. Drummond, D. B. A. Jones, Z. Cao, H. Bremer, J. Kar, J. Zou, F. Nichitiu, and J. C.  
31 | Gille, Large horizontal gradients in atmospheric CO at the synoptic scale as seen by spaceborne  
32 | Measurements of Pollution in the Troposphere, *J. Geophys. Res.*, 111, D02306,  
33 | doi:10.1029/2005JD006076, 2006.

- 1 | Liu, J., J. R. Drummond, Qinbin Li, John C. Gille, Daniel C. Ziskin, Satellite mapping of CO  
2 | emission from forest fires in Northwest America using MOPITT measurements, *Remote Sens.*  
3 | *Environ.*, 95, 502–516, 2005
- 4 | Logan, J. A., M. J. Prather, S.C. Wofsy, and M. B. McElroy, Tropospheric chemistry: A global  
5 | perspective, *J. Geophys. Res.*, 86, 7210-7254, 1981.
- 6 | Luo, M., C. P. Rinsland, C. D. Rodgers, J. A. Logan, H. Worden, S. Kulawik, A. Eldering, A.  
7 | Goldman, M. W. Shephard, M. Gunson, and M. Lampel, Comparison of carbon monoxide  
8 | measurements by TES and MOPITT: Influence of a priori data and instrument characteristics on  
9 | nadir atmospheric species retrievals, *J. Geophys. Res.*, 112, D09303,  
10 | doi:10.1029/2006JD007663, 2007.
- 11 | Marenco, A., Thouret, V., Nédélec, P., Smit, H., Helten, M., Kley, D., Karcher, F., Simon, P.,  
12 | Law, K., Pyle, J., Poschmann, G., Wrede, R. V., Hume, C., and Cook, T.: Measurements of  
13 | ozone and water vapour by Airbus in-service aircraft: The MOZAIC airborne program, An  
14 | overview, *J. Geophys. Res.*, 103, 25631–25642, 1998.
- 15 | Mauzerall, D. L., D. J. Jacob, S.-M. Fan, J. D. Bradshaw, G. L. Gregory, G. W. Sachse, and D.  
16 | R. Blake, Origin of tropospheric ozone at remote high northern latitudes in summer, *J. Geophys.*  
17 | *Res.*, 101, 4175–4188, 1996.
- 18 | Mauzerall, D. L., D. Narita, H. Akimoto, L. Horowitz, S. Walters, D. A. Hauglustaine, and G.  
19 | Brasseur, Seasonal characteristics of tropospheric ozone production and mixing ratios over East  
20 | Asia: A global three dimensional chemical transport and model analysis, *J. Geophys. Res.*, 105,  
21 | 17,895– 17,910, 2000.
- 22 | McKee, D. J. (Ed.): *Tropospheric Ozone: Human Health and Agricultural Impacts*, Boca Raton,  
23 | Fla.: Lewis Publishers, 39-208, 1993.
- 24 | [Nédélec, Nedelee](#) P., Cammas J. P., Thouret V., Athier G., Cousin J. M., Legrand C., Abonnel C.,  
25 | Lecoeur F., Cayez G. and Marizy C., An Improved Infra-Red Carbon Monoxide Analyser for  
26 | Routine Measurements aboard Commercial Airbus Aircraft : Technical Validation and First  
27 | Scientific Results of the MOZAIC III Program, *Atmos. Chem. And Phys.*, Vol. 3, pp 1551-1564,  
28 | 2003.
- 29 | Nédélec P., Thouret V., Brioude J., Sauvage B., and Cammas J.-P., Sthol A. : Extreme CO  
30 | concentrations in the upper troposphere over North-East Asia in June 2003 from the in-situ  
31 | MOZAIC aircraft data. *Geophysical Research Letters*, 32, L14807, doi:10.1029/2005GL023141,  
32 | 2005.
- 33 | Nédélec, P., R. Blot, D. Boulanger, G. Athier, J.-M. Cousin, B. Gautron, A. Petzold, A. Volz-  
34 | Thomas and V. Thouret, Instrumentation on commercial aircraft for monitoring the atmospheric  
35 | composition on a global scale: the IAGOS system, technical overview of ozone and carbon

1 monoxide measurements, *Tellus B*, 67, 27791, <http://dx.doi.org/10.3402/tellusb.v67.27791>,  
2 2015.

3 Novelli, P. C., L. P. Steele, and P. P. Tans, Mixing ratios of carbon monoxide in the troposphere.  
4 *J. Geophys. Res.*, 97, 20,731-20,750, 1992.

5 | Novelli, P. C., K. A. Masarie, P. P. Tans, and P. M. Lang, Recent changes in atmospheric carbon  
6 monoxide, *Science*, 263, 1587-1590, 1994.

7 | Novelli, P. C., K. A. Masarie, P. M. Lang, B. D. Hall, R. C. Myers, and J. W. Elkins, Reanalysis  
8 of tropospheric CO trends: Effects of the 1997–1998 wildfires, *J. Geophys. Res.*, 108(D15),  
9 4464, doi:10.1029/2002JD003031, 2003.

10 | Novelli, P. C., Masarie, K. A., Lang, P. M., Distributions and recent changes of carbon monoxide  
11 in the lower troposphere, *J. Geophys. Res.*, 103 (D51), 19015–19033, 1998.

12 | Osman, M., D. W. Tarasick, J. Liu, V. Thouret, V. E. Fioletov, O. Moeini, C. McLinden, C.  
13 Sioris, M. Parrington and P. Nédélec: Ozone climatology derived from the Trajectory Mapping  
14 of Global aircraft (MOZAIC-IAGOS), satellite (ACE-FTS, SAGE) and extended ozonesonde  
15 data, in preparation, 2016.

16 | Pan, L. L., Konopka, P., and Browell, E. V.: Observations and model simulations of mixing near  
17 the extratropical tropopause, *J. Geophys. Res.*, 111(D05106), doi:10.1029/2005JD006480, 2006.

18 | Parrish, D. D., M. Trainer, J. S. Holloway, J. E. Yee, M. S. Warshawsky, F. C. Fehsenfeld, G. L.  
19 Forbes, and J. L. Moody, Relationships between ozone and carbon monoxide at surface sites in  
20 the North Atlantic region, *J. Geophys. Res.*, 103, 13,357– 13,376, 1998.

21 | Parrish, D. D., M. Trainer, M. P. Buhr, B. A. Watkins, and F. C. Fehsenfeld, Carbon monoxide  
22 concentrations and their relation to concentrations of total reactive oxidized nitrogen at two rural  
23 U.S. sites, *J. Geophys. Res.*, 96, 9309-9320, 1991.

24 | Petetin, H., Thouret, V., Fontaine, A., Sauvage, B., Athier, G., Blot, R., Boulanger, D., Cousin,  
25 J.-M., and Nédélec, P.: Characterizing tropospheric ozone and CO around Frankfurt between  
26 1994–2012 based on MOZAIC-IAGOS aircraft measurements, *Atmos. Chem. Phys. Discuss.*,  
27 15, 23841-23891, doi:10.5194/acpd-15-23841-2015, 2015.

28 | Petzold, A., V. Thouret, C. Gerbig, A. Zahn, C. A. M. Brenninkmeijer, M. Gallagher, M.  
29 Hermann, M. Pontaud, H. Ziereis, D. Boulanger, J. Marshall, P. Nédélec, H. G. J. Smit, U. Frieß,  
30 J.-M. Flaud, A. Wahner, J.-P. Cammas, A. Volz-Thomas, and IAGOS Team, Global-scale  
31 atmosphere monitoring by in-service aircraft – current achievements and future prospects of the  
32 European research infrastructure IAGOS. *Tellus B*, 67,  
33 <http://dx.doi.org/10.3402/tellusb.v67.28452>, 2015.

Formatted: Left

Formatted: Left, Don't adjust space between Latin and Asian text

- 1 | Ploeger, F., Konopka, P., ~~Günther~~Günther, G., Grooß, J.-U., and ~~Müller~~Müller, R.: Impact of  
2 | the vertical velocity scheme on modeling transport across the tropical tropopause layer, J.  
3 | Geophys. Res., 115, D03301, doi: 10.1029/2009JD012023, 2010.
- 4 | Ploeger, F., Konopka, P., ~~Müller~~Müller, R., ~~Günther~~Günther, G., Grooß, J.-U., Schiller, C.,  
5 | Ravegnani, F., Ulanovski, A., and Riese, M.: Backtrajectory reconstruction of water vapour and  
6 | ozone in-situ observations in the TTL, Meteorol. Z., 21(3), 239–244, 2012.
- 7 | Pommrich, R., ~~Müller~~Müller, R., Grooß, J.-U., Konopka, P., Ploeger, F., Vogel, B., Tao, M.,  
8 | Hoppe, C. M., ~~Günther~~Günther, G., Spelten, N., Hoffmann, L., Pumphrey, H.-C., Viciani, S.,  
9 | D’Amato, F., Volk, C. M., Hoor, P., Schlager, H., and Riese, M.: Tropical troposphere to  
10 | stratosphere transport of carbon monoxide and long-lived trace species in the Chemical  
11 | Lagrangian Model of the Stratosphere (CLaMS), Geosci. Model Dev., 7, 2895–2916,  
12 | doi:10.5194/gmd-7-2895-2014, 2014.
- 13 | Reichle, H. G., Jr., H. G. Reichle Jr., B. E. Anderson, V. S. Connors, T. C. Denkins, D. A.  
14 | Forbes, B. B. Gormsen, R. L. Langenfelds, D. O. Neil, S. R. Nolf, P. C. Novelli, N. S.  
15 | Pougatchev, M. M. Roell, L. P. Steele., Space shuttle based global CO measurements during  
16 | April and October 1994, MAPS instrument, data reduction, and data validation, J. Geophys.  
17 | Res., 104, 21,443–21,454, 1999.
- 18 | Reichle, H. G., Jr., V. S. Connors, J. A. Holland, R. T. Sherrill, H. A. Wallio, J. C. Casas, E. P.  
19 | Condon, B. B. Gormsen, W. Seiler, The distribution of middle tropospheric carbon monoxide  
20 | during early October 1984, J. Geophys. Res., 95(D7), 9845-9856, 1990.
- 21 | Rinsland, C .P., and J.S. Levine, Free tropospheric carbon monoxide concentrations in 1950 and  
22 | 1951 deduced from infrared total column amount measurements, Nature, 318, 250-254, 1985.
- 23 | Rinsland, C. P., Jones, N. B., Connor, B. J., Wood, S. W., Goldman, A., Stephen, T. M.,  
24 | Murcray, F. J., Chiou, L. S., Zander, R. & Mahieu, E., Multiyear infrared solar spectroscopic  
25 | measurements of HCN, CO, C<sub>2</sub>H<sub>6</sub>, and C<sub>2</sub>H<sub>2</sub> tropospheric columns above Lauder, New Zealand  
26 | (45 S Latitude). J. Geophys. Res., 107 (D14), 1-12, 2002.
- 27 | Rodgers, C. D., Inverse Methods for Atmospheric Sounding: Theory and Practice, World Sci.,  
28 | Hackensack, N. J., 2000.
- 29 | Sauvage B., V. Thouret, J.-P. Cammas, F. Gheusi, G. Athier, P. Nédélec, Tropospheric ozone  
30 | over Equatorial Africa : regional aspects from the MOZAIC data. Atmospheric Chemistry and  
31 | Physics, Vol. 5, pp 311-335, 2005.
- 32 | Sauvage, B., F. Gheusi, V. Thouret, J.-P. Cammas, J. Duron, J. Escobar, C. Mari, P. Mascart, and  
33 | V. Pont, Medium-range mid-tropospheric transport of ozone and precursors over Africa: two  
34 | numerical case-studies in dry and wet seasons, Atmos. Chem. Phys., 7, 5357-5370, 2007.

Formatted: Left

- 1 Schoeberl, M. R., Douglass, A. R., Zhu, Z. X., and Pawson, S.: A comparison of the lower  
2 stratospheric age spectra derived from a general circulation model and two data assimilation  
3 systems, *J. Geophys. Res.*, 108, 4113, DOI: 10.1029/2002JD002652, 2003.
- 4 | Shindell, D.T., G. Faluvegi, D.S. Stevenson, M.C. Krol, L.K. Emmons, J.-F. Lamarque, G.  
5 Pétron, F.J. Dentener, K. Ellingsen, M.G. Schultz, O. Wild, M. Amann, C.S. Atherton, D.J.  
6 Bergmann, I. Bey, T. Butler, J. Cofala, W.J. Collins, R.G. Derwent, R.M. Doherty, J. Drevet,  
7 H.J. Eskes, A.M. Fiore, M. Gauss, D.A. Hauglustaine, L.W. Horowitz, I.S.A. Isaksen, M.G.  
8 Lawrence, V. Montanaro, J.-F. Müller, G. Pitari, M.J. Prather, J.A. Pyle, S. Rast, J.M.  
9 Rodriguez, M.G. Sanderson, N.H. Savage, S.E. Strahan, K. Sudo, S. Szopa, N. Unger, T.P.C.  
10 van Noije, and G. Zeng, Multi-model simulations of carbon monoxide: Comparison with  
11 observations and projected near-future changes. *J. Geophys. Res.*, 111, D19306,  
12 doi:10.1029/2006JD007100, 2006.
- 13 | Stein, O., M. G. Schultz, I. Bouarar, H. Clark, V. Huijnen, A. Gaudel, M. George, and C.  
14 Clerbaux, On the wintertime low bias of Northern Hemisphere carbon monoxide found in global  
15 model simulations, *Atmos. Chem. Phys.*, 14, 9295–9316, 2014.
- 16 | Stohl, A. and Seibert, P., Accuracy of trajectories as determined from the conservation of  
17 meteorological tracers, *Q. J. R. Meteorol. Soc.*, 125: 1465–1484, 1998.
- 18 | Stohl, A., Computation, accuracy and applications of trajectories - review and bibliography,  
19 *Atmos. Environ.* 32, 947-966, 1998.
- 20 | Stohl, A., James, P., Forster, C., and Spichtinger, N.: An extension of Measurement of Ozone  
21 and Water Vapour by Airbus-In-service aircraft (MOZAIC) ozone climatologies using trajectory  
22 statistics, *J. Geophys. Res.*, 106, D21, 27,757-27,768, doi:10.1029/2001JD000749, 2001.
- 23 | Tan, Q., Chameides, W. L., Streets, D., Wang, T., Xu, J., Bergin, M., and Woo, J.: An evaluation  
24 of TRACE-P emission inventories from China using a regional model and chemical  
25 measurements, *J. Geophys. Res.*, 109, D22305, doi:10.1029/2004JD005071, 2004.
- 26 | Tarasick, D. W., Jin, J. J., Fioletov, V. E., Liu, G., Tompson, A. M., Oltmans, S. J., Liu, J.,  
27 Sioris, C. E., Liu, X., Cooper, O. R., Dann, T., and Thouret, V.: High-resolution tropospheric  
28 ozone fields for INTEX and ARCTAS from IONS ozonesondes, *J. Geophys. Res.*, 115, D20301,  
29 doi:10.1029/2009JD012918, 2010.
- 30 | Thompson, A. M.: The oxidizing capacity of the Earth's atmosphere-Probable past and future  
31 changes, *Science*, 256, 1157–1165, doi:10.1126/science.256.5060.1157, 1992.
- 32 | Tie, X., G. P. Brasseur, C. Zhao, C. Granier, S. Massie, Y. Qin, P. Wang, G. Wang, P. Yang, A.  
33 Richterg, Chemical characterization of air pollution in eastern China and the eastern United  
34 States, *Atmos. Environ.*, 40, 2607–2625, 2006.

Formatted: Left



- 1 | Vogel, B., Pan, L. L., Konopka, P., ~~Günther~~Günther, G., ~~Müller~~Müller, R., Hall, W., Campos,  
2 | T., Pollack, I., Weinheimer, A., Wei, J., Atlas, E. L., and Bowman, K. P.: Transport pathways  
3 | and signatures of mixing in the extratropical tropopause region derived from Lagrangian model  
4 | simulations, *J. Geophys. Res.*, 116, D05306, doi:10.1029/2010JD014876, 2011.
- 5 | Volz-Thomas A., Berg M., Heil T., Houben N., Lerner A., Petrick W., Raak D., Pätz H. -W.,  
6 | Measurements of total odd nitrogen (NO<sub>y</sub>) aboard MOZAIC in-service aircraft: instrument  
7 | design, operation and performance, *Atmospheric Chemistry and Physics*, Vol. 5, pp 583-595,  
8 | 2005
- 9 | Wang, T., K. S. Lam, L. Y. Chan, M. A. Carroll, A. S.Y. Lee, Trace gas measurements in coastal  
10 | Hong Kong during the PEM-WEST (B), *J. Geophys. Res.* Vol. 102, 28,575-28,588, 1997.
- 11 | Wang, T., M. A. Carroll, G. M. Alber, K. R. Owens, K. A. Duderstadt, and A. Markevitch, D.  
12 | Parrish, J. Holloway, and F. C. Fehsenfeld, G. Forbes and J. Ogren, Ground-based measurements  
13 | of NO<sub>x</sub> and total reactive oxidized Nitrogen (NO<sub>y</sub>) at Sable Island, Nova Scotia during the  
14 | NARE 1993 Summer Intensive, *J. Geophys. Res.*, 101, 28,991-29,004, 1996
- 15 | Wang, Y. X., McElroy, M. B., Wang, T., and Palmer, P. I.: Asian emissions of CO and NO<sub>x</sub>:  
16 | Constraints from aircraft and Chinese station data, *J. Geophys. Res.*, 109, D24304,  
17 | doi:10.1029/2004JD005250, 2004.
- 18 | WHO, Air quality guidelines for Europe, 2nd ed. Copenhagen, World Health Organization  
19 | Regional Office for Europe, 2000 (WHO Regional Publications, European Series No. 91), 2000
- 20 | Worden, H. M., Deeter, M. N., Edwards, D. P., Gille, J. C., Drummond, J. R., and Ned'elec, P.  
21 | P.: Observations of near-surface carbon monoxide from space using MOPITT multispectral  
22 | retrievals, *J. Geophys. Res.*, 115, D18314, doi:10.1029/2010JD014242, 2010.
- 23 | Worden, H. M., M. N. Deeter, C. Frankenberg, M. George, F. Nichitiu, J. Worden, I. Aben, K.  
24 | W. Bowman, C. Clerbaux, P. F. Coheur, A. T. J. de Laat, R. Detweiler, J. R. Drummond, D. P.  
25 | Edwards, J. C. Gille, D. Hurtmans, M. Luo, S. Martínez-Alonso, S. Massie, G. Pfister, and J. X.  
26 | Warner,, Decadal record of satellite carbon monoxide observations, *Atmos. Chem. Phys.*, 13,  
27 | 837–850, doi:10.5194/acp-13-837-2013, 2013.
- 28 | Yurganov, L. N., McMillan, W., Dzhola, A. V., Grechko, E. I., Jones, N. B. & van der Werf, G.  
29 | R., Global AIRS and MOPITT CO measurements: validation, comparison, and links to biomass  
30 | burning variations and carbon cycle. *J. Geophys. Res.*, 113 (D9), 1-14, 2008).
- 31 | Zander, R., P. Demoulin, D.H. Ehhalt, U. Schmidt, and C.P. Rinsland, Secular increase of the  
32 | total vertical column abundance of carbon monoxide above central Europe since 1950, *J.*  
33 | *Geophys. Res.*, 94, 11, 021-11,028, 1989.

Formatted: Left

- 1 | Zbinden, R. M., V. Thouret, P. Ricaud, F. Carminati, J.-P. Cammas, P. Nédélec, Climatology of  
2 | pure tropospheric profiles and column contents of ozone and carbon monoxide using MOZAIC  
3 | in the mid-northern latitudes (24° N to 50° N) from 1994 to 2009, doi:10.5194/acp-13-12363-  
4 | 2013, 2013.
- 5 | Zeng, G., Wood, S. W., Morgenstern, O., Jones, N. B., Robinson, J. & Smale, D., Trends and  
6 | variations in CO, C<sub>2</sub>H<sub>6</sub>, and HCN in the Southern Hemisphere point to the declining  
7 | anthropogenic emissions of CO and C<sub>2</sub>H<sub>6</sub>, Atmos. Chem. Phys., 12 (16), 7543-7555, 2012.
- 8 | Zhang, L., Jacob, D. J., Liu, X., Logan, J. A., Chance, K., Eldering, A., and Bojkov, B. R.:  
9 | Intercomparison methods for satellite measurements of atmospheric composition: application to  
10 | tropospheric ozone from TES and OMI, Atmos. Chem. Phys., 10, 4725–4739, doi:10.5194/acp-  
11 | 10-4725-2010, 2010.

12 |